Modeling the observed tropospheric BrO background: Importance of multiphase chemistry and implications for ozone, OH, and mercury

J. A. Schmidt,[1,2] D. J. Jacob,[1,3] H. M. Horowitz,[3] L. Hu,[1] T. Sherwen,[4] M. J. Evans,[4] Q. Liang,[5] R. M. Suleiman,[6] D. E. Oram,[7] M. Le Breton,[8] C. J. Percival,[8] S. Wang,[9,10,11] B. Dix,[10] and R. Volkamer,[10,11]

Recent tropospheric BrO observations are interpreted using a new GEOS-Chem coupled Br-Cl simulation.

Multi-phase oxidation of bromide by ozone is critical for maintaining the high observed levels of BrO in the upper troposphere.

Br and Cl lower the global burden of ozone by 14 %, by increasing NO_x loss and shortening the lifetime of ozone.

Corresponding author: J. A. Schmidt, Department of Chemistry, Copenhagen University, Universitetsparken 5, DK-2100 Copenhagen O, Denmark. (schmidt@chem.ku.dk)

[1]Harvard University, School of Engineering and Applied Sciences, 29 Oxford St., Cambridge, MA 02138, USA

[2]University of Copenhagen, Department of Chemistry, Universitetsparken 5, Copenhagen, DK-2100, Denmark

Abstract. Aircraft and satellite observations indicate the presence of ppt (ppt ≡ pmol/mol) levels of BrO in the free troposphere with important

[3]Harvard University, Department of Earth and Planetary Sciences, 20 Oxford St., Cambridge, MA 02138, USA

[4]Wolfson Atmospheric Chemistry Laboratories (WACL), Department of Chemistry, University of York, York, YO10 5DD, UK

[5]NASA Goddard Space Flight Center, Laboratory for Atmospheric Chemistry and Dynamics, Greenbelt, MD 20771, USA

[6]Harvard Smithsonian Center for Astrophysics, 60 Garden St., Cambridge, MA 02138, USA

[7]Centre for Oceanography and Atmospheric Science, National Centre for Atmospheric Science, University of East Anglia, Norwich, NR4 7TJ, UK.

[8]The Centre for Atmospheric Science, School of Earth, Atmospheric and Environmental Sciences, University of

implications for the tropospheric budgets of ozone, OH, and mercury. We can reproduce these observations with the GEOS-Chem global tropospheric chemistry model by including a broader consideration of multiphase halogen (Br–Cl) chemistry than has been done in the past. Important reactions for regenerating BrO from its non-radical reservoirs include $HOBr+Br^-/Cl^-$ in both aerosols and clouds, and oxidation of Br^- by $ClNO_3$ and ozone. Most tropospheric BrO in the model is in the free troposphere, consistent with observations, and originates mainly from the photolysis and oxidation of ocean-emitted $CHBr_3$. Stratospheric input is also important in the upper troposphere. Including production of gas phase inorganic bromine from debromi-

Manchester, Brunswick St., Manchester, M13 9PL, UK

[9]Department of Chemistry, University of Michigan, 930 N. University Ave., Ann Arbor, MI 48109, USA

[10]Department of Chemistry and Biochemistry, University of Colorado, Boulder, CO 80309, USA

[11]Cooperative Institute for Research in Environmental Sciences, University of Colorado, Boulder, CO 80309, USA

nation of acidified sea salt aerosol increases free tropospheric Br_y by about 30 %. We find HOBr to be the dominant gas-phase reservoir of inorganic bromine. Halogen (Br-Cl) radical chemistry as implemented here in GEOS-Chem drives 14 % and 11 % decreases in the global burdens of tropospheric ozone and OH, respectively, a 16 % increase in the atmospheric lifetime of methane, and an atmospheric lifetime of 6 months for elemental mercury. The dominant mechanism for the Br-Cl driven tropospheric ozone decrease is oxidation of NO_x by formation and hydrolysis of $BrNO_3$ and $ClNO_3$.

1. Introduction

Atmospheric bromine radicals (BrO_x≡Br+BrO) destroy ozone, perturb HO_x (OH + HO_2) and NO_x (NO + NO_2) radical budgets, and provide a sink for mercury [*von Glasow et al.*, 2004; *Parrella et al.*, 2012; *Simpson et al.*, 2015]. The importance of bromine radical chemistry is well established in the stratosphere [*Montzka et al.*, 2010] and in the Arctic boundary layer in spring [*Barrie et al.*, 1988; *Simpson et al.*, 2007]. There is increasing evidence for a tropospheric background BrO concentration of the order of 1 ppt (ppt = pmol/mol) in the daytime [*Platt and Hönninger*, 2003; *Sinnhuber et al.*, 2005; *Prados-Roman et al.*, 2011; *Theys et al.*, 2011; *Volkamer et al.*, 2015; *Wang et al.*, 2015]. Such a background would provide a major sink for tropospheric ozone and also deplete OH, the main tropospheric oxidant [*von Glasow et al.*, 2004; *Yang et al.*, 2005; *Saiz-Lopez et al.*, 2012; *Parrella et al.*, 2012; *Wang et al.*, 2015]. It would also imply atomic Br concentrations sufficiently high to provide the main oxidant for gaseous elemental mercury and thus drive the patterns of mercury deposition to ecosystems [*Holmes et al.*, 2010; *Wang et al.*, 2015; *Gratz et al.*, 2015; *Coburn et al.*, 2016]. Here we use a global 3-D chemical transport model (GEOS-Chem CTM) to interpret recent observations of tropospheric BrO and its reservoirs in terms of our understanding of tropospheric bromine chemistry and its implications.

The main sources of reactive inorganic bromine (Br_y) in the troposphere are photochemical decomposition of organobromines ($CHBr_3$, CH_2Br_2, CH_3Br), release of bromine from sea salt aerosol (SSA), and transport from the stratosphere where Br_y originates from photochemical decomposition of organobromines and halons [*Yang et al.*, 2005; *Liang et al.*,

2014]. CH_2Br_2 and $CHBr_3$ are of marine biogenic origin, while CH_3Br has both natural and anthropogenic sources [*Montzka et al.*, 2010]. Cycling of Br_y takes place between BrO_x radicals and non-radical reservoirs (including HBr, HOBr, $BrNO_2$, $BrNO_3$, Br_2, BrCl). Br_y is eventually removed from the troposphere by dry and wet deposition.

A number of global model studies have pointed out the potential importance of BrO_x radicals for global tropospheric chemistry [*von Glasow et al.*, 2004; *Yang et al.*, 2005; *Warwick et al.*, 2006; *Breider et al.*, 2010; *Hossaini et al.*, 2010; *Parrella et al.*, 2012; *Ordóñez et al.*, 2012; *Saiz-Lopez et al.*, 2012; *Long et al.*, 2014; *Fernandez et al.*, 2014; *Sherwen et al.*, 2016]. Confidence in these models has been limited by the paucity of observational constraints on BrO and other Br_y species. The previous GEOS-Chem study by *Parrella et al.* [2012] underestimated GOME-2 satellite observations of tropospheric BrO columns by $\sim$ 30%. Model predictions for BrO in the tropical upper troposphere [*Yang et al.*, 2005; *Parrella et al.*, 2012; *Long et al.*, 2014; *Fernandez et al.*, 2014] are much smaller than recent observations [*Volkamer et al.*, 2015; *Wang et al.*, 2015]. Here we use new aircraft observations of BrO, together with BrO observations from satellites, to better constrain tropospheric bromine chemistry in models. We propose in particular that the coupling of bromine reservoirs (HBr/Br^- and HOBr) to chlorine and ozone through multiphase chemistry is more important than previously recognized for sustaining the high observed levels of BrO and Br_y in the troposphere.

2. Model description

We use the GEOS-Chem global CTM (v9-02; http://www.geos-chem.org) including a detailed ozone-NOx-VOC-aerosol-Br-Cl tropospheric chemistry mechanism. The model is driven by GEOS-5 assimilated meteorological data from the NASA Global Modeling and

Assimilation Office with $1/2^\circ \times 2/3^\circ$ horizontal resolution and 47 vertical layers extending from the surface up to 80 km. The horizontal resolution is degraded here to $4^\circ \times 5^\circ$ for input to GEOS-Chem. The year 2007 is chosen as a reference and all simulations are spun-up over 1 year (2006) for initialization.

The simulation updates the tropospheric bromine mechanism originally described by *Parrella et al.* [2012], to include a more extensive multiphase chemistry mechanism as described below. We have also added a simulation of tropospheric chlorine radical chemistry coupled to that of bromine as providing an important pathway for recycling of bromine radicals. For the purpose of this paper we define Br_y and Cl_y as the reactive inorganic halogens, excluding halide contained in sea salt that has not yet been activated to produce gas-phase inorganic halogen species.

The sources of reactive tropospheric inorganic halogens are listed in Table 1. Production from organohalogens by oxidation and photolysis is well established. Our simulation of organobromines is as in *Parrella et al.* [2012], who showed good agreement with vertical profiles observed from aircraft campaigns. We confirm this agreement in model comparisons to aircraft observations of organobromines from the CARIBIC project covering the upper troposphere [*Wisher et al.*, 2014, see also http://www.caribic-atmospheric.com], the TORERO campaign covering the Eastern Pacific, and HIPPO campaign across the Pacific [*Wofsy et al.*, 2012a, b], see Fig. S1 in Supporting Information (SI). CH_3Br+OH kinetics are updated according to *Nilsson et al.* [2013], increasing the Br_y source contribution by tropospheric CH_3Br from $56\,\mathrm{Gg\,Br\,a^{-1}}$ in *Parrella et al.* [2012] to $91\,\mathrm{Gg\,Br\,a^{-1}}$ here. This remains small compared to the dominant organobromine source from $CHBr_3$ ($404\,\mathrm{Gg\,Br\,a^{-1}}$). Stratospheric Br_y is treated as a boundary condition above the GEOS-5

tropopause using archived Br_y fields from the GEOSCCM global 3-D simulation by *Liang et al.* [2010] that are consistent with balloon based stratospheric BrO observations [*Liang et al.*, 2014].

Additional generation of bromine radicals by oxidation of bromide in SSA is uncertain and highly variable. Observations in the marine boundary layer (MBL) generally show BrO below the detection limit of ≤ 1 ppt [*Leser et al.*, 2003; *Gomez Martin et al.*, 2013; *Volkamer et al.*, 2015; *Wang et al.*, 2015], but some studies show detectable higher values [*Saiz-Lopez et al.*, 2004; *Read et al.*, 2008; *Martin et al.*, 2009]. The underlying mechanisms are poorly understood and could be sensitive to a number of factors including aerosol acidity and the presence of dissolved organic matter [*Fickert et al.*, 1999; *Liang and Singer*, 2003]. We perform two seperate simulations (A and B): Our simulation A does not include dehalogenation of SSA. Our simulation B includes dehalogenation of acidic SSA as a source of Br_y and Cl_y. The GEOS-Chem SSA simulation is as described by *Jaegle et al.* [2011] and sea salt bromide (Br^-_{SSA}) is emitted as part of SSA with a ratio of 2.11×10^{-3} kg Br (kg dry SSA)$^{-1}$ [*Lewis and Schwartz*, 2004]. The transport and deposition of Br^-_{SSA} follows that of the parent sea salt aerosol. Release of Br_2, BrCl and HOBr from acidified SSA follows the general multiphase chemistry mechanism described below. Uptake of gas-phase HBr by SSA provides an additional source of Br^-_{SSA}.

Removal of Br_y and Cl_y takes place by wet and dry deposition. Wet deposition of gases and aerosols follows the schemes described by *Amos et al.* [2012] and *Wang et al.* [2011], respectively. Dry deposition is computed with the resistance-in-series scheme of *Wesely* [1989] as implemented by *Wang et al.* [1998]. Deposition of gases depends on the Henry's law and acid dissociation constants.

2.1. Tropospheric chlorine simulation

The chlorine simulation is based on the GEOS-Chem UCX chlorine mechanism for the stratosphere [*Eastham et al.*, 2014] extended here to the troposphere. Sources of reactive inorganic tropospheric chlorine (Cl_y) include oxidation of organochlorines, release from sea salt (in simulation B), and transport from the stratosphere (Table 1). We add 14 gas phase chlorine species to the GEOS-Chem tropospheric mechanism: BrCl, Cl_2, Cl, ClO, HCl, HOCl, $ClNO_2$, $ClNO_3$, ClOO, OClO, Cl_2O_2, CH_3Cl, CH_2Cl_2, and $CHCl_3$.

The organochlorines release atomic Cl when oxidized by OH and Cl. Their sources are represented implicitly by imposing fixed surface mixing ratios of 550 ppt CH_3Cl, 20 ppt CH_2Cl_2, and 7 ppt $CHCl_3$ based on 2007 NOAA and AGAGE network data [*Montzka et al.*, 2010]. The model lifetimes of these organochlorines against oxidation are 480, 158 and 152 days, respectively, which implies that CH_3Cl is the dominant source of inorganic chlorine in the standard simulation (See Table 1). Chlorine is released from SSA in simulation B through the multiphase chemistry mechanism described below. We do not consider acid displacement of HCl from sea salt nor chloride activation by N_2O_5. The latter mechanism can drive large chlorine release in polluted continental regions [*Thornton et al.*, 2010] but we expect it to be of little importance globally. Stratospheric chlorine is simulated following *Murray et al.* [2012] by using archived monthly mean production and loss rate constants for individual chlorine species from the Global Modeling Initiative (GMI) stratospheric model.

2.2. Halogen multiphase chemistry

Our halogen multiphase chemistry mechanism (halogen X≡ Br or Cl) is based on recommendations by IUPAC [*Ammann et al.*, 2013] and takes place in liquid and ice clouds, sea

salt aerosol, and sulfate aerosol (the implementation of sulfate aerosols in GEOS-Chem is described by *Park et al.* [2004] and *Pye et al.* [2009]). The mechanism includes hydrolysis of halonitrates,

$$XNO_3 \xrightarrow{H_2O} HOX + HNO_3,$$

and oxidation of halides by HOBr, $ClNO_3$ and O_3,

$$HOBr + X^- + H^+ \longrightarrow BrX + H_2O,$$

$$ClNO_3 + Br^- \longrightarrow BrCl + NO_3^-,$$

$$O_3 + Br^- \xrightarrow{H_2O} HOBr + OH^- + O_2.$$

The rate of reaction depends on the concentration of gas-phase reactant, $[A(g)]$, and condensed phase surface area concentration, $[S]$, following the parameterization from *Ammann et al.* [2013],

$$\frac{d[A(g)]}{dt} = -\gamma \frac{c}{4}[S][A(g)], \quad (1)$$

where γ is the reactive uptake coefficient and c is the mean thermal velocity of A. The reactive uptake coefficient as defined here includes all mass transfer limitations. It is calculated following a resistor-in-series expression,

$$\frac{1}{\gamma} = \frac{1}{\gamma_d} + \frac{1}{\gamma'} \quad (2)$$

where $1/\gamma_d$ is the resistance to gas-phase diffusion that depend on the particle radius (r) and the gas-phase diffusion coefficient of A in air ($D_{A,g}$),

$$\gamma_d = \frac{4\,D_{A,g}}{c\,r}. \quad (3)$$

$1/\gamma'$ is the total condensed-phase resistance to subsequent mass accommodation, mass transfer, and first-order reaction. It depends on a number of factors including particle radius, particle halide concentration, pH and temperature, as described in Tables 2 and 3. In addition, we include uptake of HBr on SSA to form Br^-_{SSA} with $\gamma' = 1.3 \times 10^{-8} \exp(4290\,\mathrm{K/T})$.

Generation of volatile dihalogens from the aqueous-phase reaction of HOBr with bromide and chloride (R1) is pH-dependent and requires acidic conditions [*Fickert et al.*, 1999]. Cloudwater pH (typically in range of 4 to 6) is calculated locally in GEOS-Chem following *Alexander et al.* [2012]. Sulfate aerosol is assumed to have a pH of 0 following the observations by *Froyd et al.* [2009] who found sulfate aerosol in the free troposphere to be strongly acidic (pH$<$ 1). Sulfate aerosol in the MBL is also prevailingly acidic [*Paulot et al.*, 2015]. Sea salt aerosol is emitted alkaline, but the alkalinity can be titrated in GEOS-Chem by uptake of HNO_3, SO_2 and H_2SO_4 [*Alexander et al.*, 2005]. Sea salt aerosol with retained alkalinity is assumed to have pH= 8 (similar to sea water), while sea salt aerosol with no remaining alkalinity is assumed to have a pH of 5. In simulation B sea salt dehalogenation is enabled for acidic SSA.

The cloud droplet and sulfate aerosol halide concentration, $[X^-]$, is modeled assuming local equilibrium between gas phase HX and condensed phase X^-. We model the surface area concentration of liquid and ice clouds using local liquid and ice water contents (LWC and IWC) from the GEOS-5 meteorological data and assuming effective radii of 10 μm and 75 μm, respectively. Studies of ice crystals have shown the existence of an unfrozen overlayer coating the droplets, in which halogens accumulate as they are expelled from the ice lattice [*Bogdan et al.*, 2006, 2010]. The thickness of this layer is typically 10^{-3} to

10^{-2} of the ice crystal diameter; in the present simulation we assume a constant value of 10^{-2}. Ice cloud multiphase chemistry is assumed to be confined to this layer.

3. Global distribution of tropospheric bromine

Figure 1 (upper panel) shows the GEOS-Chem simulated annual budget of tropospheric inorganic bromine, for the simulation not including SSA dehalogenation (simulation A). The total Br_y concentration is 7 % less than the previous GEOS-Chem simulation by *Parrella et al.* [2012]. That study included a sea salt debromination source based on observed bromide depletion factors [*Sander et al.*, 2003], with a corresponding global Br_y source from sea salt debromination of 1420 $Gg\,Br\,a^{-1}$ that is similar to the source of 1620 $Gg\,Br\,a^{-1}$ in our simulation B that includes dehalogenation of acidic SSA (Table 1). However, the geographic distribution of SSA debromination is different; *Parrella et al.* [2012] found debromination over the Southern Ocean to dominate due to high emission sea salt in this region, whereas we find less debromnination in this region as acid input are often insufficient to compensate for the high alkalinity flux. Our simulation including SSA debromination show highest levels of BrO in the MBL over the tropical and North Atlantic, where SSA alkalinity is generally fully titrated. We find a 4 fold increase in Br_y in the MBL when SSA debromination is included. The effect of SSA debromination on the free troposphere is smaller, increasing Br_y by about 30 % (Fig. 1). Approximately 1/4 of free tropospheric Br_y in the sensitivity simulation can be attributed to SSA debromination, the dominant source of Br_y in the free troposphere are photochemical oxidation of $CHBr_3$ and input from the stratosphere. HOBr is the dominant daytime Br_y species. BrCl and $BrNO_3$ are the dominant nighttime species. Overall, total Br_y show almost no diurnal variability.

The mean tropospheric BrO concentration in our simulation A is 0.48 ppt (0.96 ppt in daytime), 50 % higher than *Parrella et al.* [2012] and more consistent with the observed range as shown below. The higher BrO/Br_y ratio reflects the more efficient multiphase HBr recycling. HBr accounts for only 6 % of Br_y in our simulation, as compared to 34 % in *Parrella et al.* [2012]. Cycling of HBr in our simulation is faster as we include bromide oxidation by HOBr in liquid cloud droplets and by $ClNO_3$ and O_3, not considered in *Parrella et al.* [2012]. We find that $BrNO_3$ is a more important Br_y reservoir as aqueous-phase $BrNO_3$ hydrolysis in our simulation ($\gamma' = 0.02$) is considerably slower than in *Parrella et al.* [2012] ($\gamma' = 0.3$ for clouds and sea salt and $\gamma' = 0.8$ for sulfate aerosol).

The model study of *Long et al.* [2014] found Br_2 and BrCl to be the dominant tropospheric Br_y species globally, and the study of *Fernandez et al.* [2014] found HBr to dominate. We find HOBr to be the dominant Br_y reservoir globally (Fig. 1), except in the upper troposphere where HOBr formation by the BrO + HO_2 reaction is suppressed by low levels of HO_2 (See Figs. S4 and S5). BrCl is the dominant nighttime Br_y reservoir, produced by the $HOBr+Cl^-$ multiphase reaction, but $BrNO_3$ becomes increasingly important in the upper troposphere due to increasing levels of NO_x and lower levels of HOBr. BrCl has no chemical sinks at night and a mean lifetime against photolysis of 20 minutes in daytime, thus rapidly returning BrO_x radicals following sunrise.

A critical component of the mechanism for maintaining elevated BrO levels is the multiphase oxidation of bromide, as pointed out by *Parrella et al.* [2012], because HBr is otherwise long-lived against gas-phase oxidation (Fig. 1). We find that HOBr is the dominant bromide oxidizer globally. Oxidation by $ClNO_3$ is mostly important at northern mid-latitudes where it is responsible $30 - 40$ % of the total bromide recycling (Fig.

S2). The O_3+Br^- reaction dominates in the tropical and subtropical upper troposphere ($> 10\,km$). About 50 % of multiphase bromide oxidation takes place in cloud droplets with the remainder taking place in sulfate aerosol.

Figure 2 shows the global mean distributions of tropospheric Br_y and BrO (simulation A). Br_y is largest in the subsiding subtropics due to the high-altitude source from organobromine photochemistry and the lack of wet deposition. Input from the stratosphere is also a significant source in that region, accounting for most of Br_y above 7 km. BrO is relatively high in the subtropics and in the upper troposphere, reflecting the distribution of Br_y, but also shows different patterns driven by the abundance of HO_2. Thus the high levels of BrO in polar regions reflect low HO_2 levels pushing the BrO/HOBr equilibrium towards BrO (Fig. S3) Photochemical equilibrium maintains [BrO]/[Br] $\gg 1$ throughout the troposphere (Fig. 1) except in the tropical tropopause layer above 15 km where the [BrO]/[Br] ratio decreases to about unity (See SI text and Fig. S4). This decrease is driven by low temperatures and low levels of ozone in the tropical upper troposphere suppressing the $Br+O_3 \rightarrow BrO+O_2$ reaction. This enhancement of Br in the tropical upper troposphere was previously identified by *Holmes et al.* [2006] for its importance in Hg(0) oxidation, and is a consistent feature of models [*Fernandez et al.*, 2014].

The global mean distribution Br_y and BrO from the simulation B (that includes dehalogenation of acidic SSA) is shown in Fig. S8. The increase in Br_y and BrO from including SSA dehalogenation is particular strong in the Northern Hemisphere MBL. Simulated SSA in this region tend to be more depleted in bromide (Fig. S9). SSA over Southern Ocean tend to retain its alkalinity preventing dehalogenation.

4. Comparison to BrO and HOBr observations

Figure 3 compares the simulated seasonal distribution of tropospheric BrO column concentrations in different latitude bands to GOME-2 satellite observations of *Theys et al.* [2011]. Both observations and model values are for 2007. Simulation A is consistent with observations in the tropics and at mid-latitudes but too low in polar regions. The previous GEOS-Chem model study of *Parrella et al.* [2012] found a $\sim 50\,\%$ low bias in the tropics. *Theys et al.* [2011] inferred the vertical profile of tropospheric BrO in the tropics (30°S–30°N) using a cloud-slicing technique and found that over 75 % of the tropospheric BrO column is above 2 km. Both simulations (A and B) are consistent with this finding (Fig. 1). Observations in the extratropical northern hemisphere show a summer minimum that was well simulated by *Parrella et al.* [2012] as due to seasonality in the SSA source. Our simulation including SSA dehalogenation captures this observed seasonal variation but is overall too high.

Figure 4 compares model results to the total BrO column observed by the OMI satellite instrument (including the stratosphere) as a function of latitude. The simulated total BrO column includes GEOS-Chem tropospheric BrO plus GEOSCCM stratospheric BrO from *Liang et al.* [2010], that serves as upper boundary condition for GEOS-Chem. We find close agreement with observations. Tropospheric BrO contributes between 25 % and 55 % of the total BrO column. Both GEOS-Chem and observations show lowest values in regions of tropical upwelling, where tropospheric Br_y is efficiently scavenged, although this is exaggerated in GEOS-Chem.

The first vertically resolved detection of tropospheric BrO in the tropical troposphere was demonstrated by the University of Colorado Airborne MAX-DOAS (CU AMAX-

DOAS) during the TORERO aircraft and ship campaign over the East Pacific [January – February 2012; *Volkamer et al.*, 2015]. Model results sampled along all 17 flight tracks are compared to observations in Fig. 5, separating tropical from subtropical flights. No BrO was detected in the MBL over the tropical Eastern Pacific. The upper limit BrO concentration is smaller than 0.5 ppt, the detection limit of CU AMAX-DOAS and Ship MAX-DOAS over the open ocean during TORERO [*Volkamer et al.*, 2015], and long-path DOAS observations at Galapagos Island during CHARLEX [*Gomez Martin et al.*, 2013]. BrO increases with altitude (0.7 to 1 ppt, between $4-8$ km) and reaches values of $1-2.5$ ppt in the upper troposphere ($8-13$ km) [*Volkamer et al.*, 2015; *Wang et al.*, 2015].

Simulation A matches closely the observed vertical profile in both the tropics and subtropics. Including SSA debromination, as in simulation B, does not change BrO in the subtropics because the model SSA in that region tends to be alkaline. However, the simulation with active sea salt dehalogenation finds about 1 ppt of BrO in tropical MBL, where SSA is simulated to be acidic. Such elevated BrO is inconsistent with the available observations [*Gomez Martin et al.*, 2013; *Volkamer et al.*, 2015]. The reason for this difference is currently not clear, but points to either overestimated sources or missing bromine sinks over the Eastern Pacific ocean. High BrO in the upper troposphere includes a dominant stratospheric component as discussed in Section 3 but also a 30 % contribution from tropospheric multiphase chemistry involving the O_3+Br^- reaction in ice cloud droplets and sulfate aerosol (Fig. S2). The oxidation of bromide by ozone is particularly important in the upper troposphere because ozone concentrations are high and HOBr concentrations are low.

A subset of the TORERO BrO observations has recently been compared with models [*Wang et al.*, 2015]. Notably, the BrO concentration was found to be variable. Slightly lower BrO was observed during case studies with pollution influences. The BrO concentration was generally higher in the pristine free troposphere, see Fig. 10 of *Volkamer et al.* [2015]. To account for atmospheric variability, *Wang et al.* [2015] compared models with average tropical and subtropical profiles in the pristine free troposphere, and not individual profile case studies. Figure S7 compares the updated model results for the subset of case studies evaluated by *Wang et al.* [2015]. We find close agreement between model and observation in the subtropics. In the tropics, the model output for the selected case studies is very similar to the overall campaign average profile shown in Fig. 5, but is less successful at reproducing the vertical gradient of BrO observed during these tropical case studies, as manifested by a low bias in the tropical upper troposphere (above 8 km). *Wang et al.* [2015] found good agreement for BrO in the lower stratosphere, and noted the negligence of models to represent bromine sources from SSA in the tropical upper free troposphere. They further suggested missing multiphase chemistry involving the O_3+Br^- reaction during deep convective lofting of sea salt aerosols, debromination of ice cloud crystals, or overestimated wet-scavenging by the model as possible reasons for the elevated BrO in the tropical upper free troposphere.

5. Implications for tropospheric ozone, OH, and mercury

Table 4 shows the GEOS-Chem global annual budget of tropospheric ozone, with and without halogen (Br-Cl) chemistry in our simulation A, compared to previous model studies. The budget of ozone is given as that of odd oxygen ($O_x \equiv O_3 + O + NO_2 + 2NO_3 +$ peroxyacylnitrates $+ HNO_3 + HNO_4 + 3N_2O_5 + XO + HOX + XNO_2 +$

266 $2XNO_3 + 2Cl_2O_2 + 2OClO$) to account for rapid cycling between O_x species. Budget
267 terms are close to those of *Parrella et al.* [2012] and in the range of the model literature
268 [*Wu et al.*, 2007]. Halogen chemistry lowers the global tropospheric ozone burden by
269 14 %, which is much larger than the 6.5 % found in the previous GEOS-Chem study by
270 *Parrella et al.* [2012]. We find that the decrease in ozone is driven by a 10 % decrease
271 in the chemical production of ozone due to lower levels of NO_x, and a 5.6 % decrease in
272 the lifetime of ozone due to halogen driven catalytic ozone loss. The finding that the
273 halogen-driven decrease in tropospheric ozone is caused by decreased NO_x-driven ozone
274 production combined with enhanced ozone destruction is consistent with previous model
275 studies [*von Glasow et al.*, 2004; *Parrella et al.*, 2012; *Long et al.*, 2014].

Halogen-driven NO_x loss takes place by hydrolysis of the halogen nitrates:

$$XO + NO_2 + M \longrightarrow XNO_3 + M$$

$$XNO_3 + H_2O(\text{droplet}) \longrightarrow HOX + HNO_3,$$

276 and decreases the global burden of tropospheric NO_x by about 6 %. Hydrolysis of $BrNO_3$
277 and $ClNO_3$ contribute equally to NO_x loss. The rate of halogen driven NO_x loss is about
278 one fifth of the rate of NO_x loss by NO_2+OH. The relative decrease in NO_x is largest
279 in low-NO_x areas such as the tropical free troposphere and polar regions (Fig. 6). By
280 contrast, NO_x increases in continental boundary layers. Here levels of reactive inorganic
281 halogens are relatively low. The decrease in the level of ozone (and OH) increase the
282 chemical lifetime of NO_x these regions.

283 Figure 7 summarizes the relative contributions of different processes to ozone destruction
284 in the tropics, where most of global tropospheric ozone loss takes place [*Wang et al.*, 1998].

The relative contribution of halogen driven ozone loss increases with altitude because of increasing BrO_x (Fig. 1). Most ozone destruction occurs below $\sim 6\,km$ (Fig. S6), where halogen chemistry drives $5-15\,\%$ of ozone loss. As previously found by *Parrella et al.* [2012] and illustrated in the lower panel of Fig. 7, Br-catalyzed ozone loss is mainly driven by HOBr formation via the $BrO+HO_2$ reaction ($87\,\%$ of total Br-catalyzed ozone loss). Chemical recycling of HOBr is important because it controls the BrO abundance. Photolysis is the dominant recycling pathway for HOBr ($71\,\%$; Fig. 7 lower panel). The multiphase $HOBr+Cl^-$ reaction drive about $15\,\%$ of HOBr recycling, and is an example of Br–Cl synergized ozone loss. $HOBr+Br^-$ is responsible for $4\,\%$ of HOBr cycling, but is critical for the cycling of bromide. The contribution of pure chlorine chemistry to chemical loss of ozone is small.

Figure 8 shows annual mean decreases in tropospheric ozone concentrations due to halogen chemistry for different regions of the troposphere. The decrease exceeds 10 ppb in the northern mid-latitude free troposphere. On average halogen chemistry decreases the tropospheric ozone column by $12\,\%$ ($2-7$ ppb) in the tropics and $17\,\%$ ($6-10$ ppb) at mid-latitudes. The large ozone decrease in the northern high-latitude free troposphere is driven by a $20-50\,\%$ decreased ozone production in this area due to lowers levels of NO_x (Fig. 6), and to a lesser extent decreased ozone lifetime due to halogen driven catalytic ozone loss. Halogen chemistry lowers surface ozone between 1 and 8 ppb: The decrease is smallest in the polluted continental PBL where halogen chemistry increases ozone production due to increased levels of NO_x (Fig. 6).

The predicted halogen driven ozone decrease in the tropics falls within previous model estimates: The study of *Saiz-Lopez et al.* [2012] found halogen chemistry (including chlo-

rine, bromine, and iodine) reduced the tropospheric ozone column by more than 10 % in the tropics. *Long et al.* [2014] found halogen (chlorine and bromine) driven ozone decreases larger than 20 % in the tropical MBL, and between 15 and 20 % in the tropical FT. *Wang et al.* [2015] found that halogen (bromine and iodine) chemistry drive 34 % of ozone loss over the over the tropical Eastern Pacific with bromine and iodine each contributing about equally. Iodine cycling has been found to contribute to halogen ozone loss in the FT and dominate in the MBL [*Saiz-Lopez et al.*, 2012; *Dix et al.*, 2013; *Wang et al.*, 2015; *Sherwen et al.*, 2016]. The GEOS-Chem based study of *Sherwen et al.* [2016] found a 9 % decrease in the global burden of ozone by introducing iodine chemistry and a halogen (bromine and iodine) driven loss comparable to this work of 14.4 %. Iodine drove a 750 Tg a^{-1} increase in the O_x loss rate and had the greatest proportional effect in the MBL and UT. *Sherwen et al.* [2016] used the bromine simulation detailed in *Parrella et al.* [2012] which results in smaller decrease in tropospheric ozone burden (6.5 %) than the 14 % from chlorine and bromine presented here. The increased BrO concentrations calculated in this work may impact the *Sherwen et al.* [2016] simulation through the coupling reaction BrO+IO. However, *Sherwen et al.* [2016], notes that the coupling in their simulation is weak. Overall, appears that both bromine and iodine have significant impacts on tropospheric composition and a coupled Cl-Br-I simulations with state of the science representations of the emissions, processing and deposition of the halogens is required to evaluate the full impact.

Previous studies have shown clear evidence for bromine-catalyzed ozone loss in observations of surface ozone in Arctic spring [*Barrie et al.*, 1988] and over the ocean [*Read et al.*, 2008]. Evidence of halogen chemistry in free tropospheric ozone observations is

more elusive because the chemical time scales are longer and effects may be masked by errors in transport, lightning NO_x emissions, or other chemical aspects. Figure 9 compares GEOS-Chem (simulation A) with and without halogen chemistry to mean ozonesonde observations in five latitudinal band [*Hu et al.*, manuscript in preparation, 2015]. Halogen chemistry lowers ozone and improves agreement with observation in the tropics and at mid-latitudes. At Northern high-latitudes ($> 50°$N) the no halogen chemistry simulated ozone profile shows very close agreement with observations and the simulation with halogen chemistry is biased low.

We find that halogen chemistry lowers global tropospheric HO_x concentrations by 5 % and OH by 11 % (Fig. 10). The effect on OH is much larger than the 4 % decrease predicted by *Parrella et al.* [2012]. The decrease in HO_x largely follows from the decrease in ozone. In addition, halogen chemistry decreases the OH/HO_2 ratio by ~ 10 % in the tropics and ~ 20 % at high latitudes: Decreased levels of NO_x results in a diminished OH-source from HO_2+NO, and the added OH-source from HOBr photolysis is too small to compensate. The model study of *Long et al.* [2014] also found halogen chemistry to decrease the OH/HO_2 ratio. The relative decrease in OH is largest at high-latitudes (~ 30 %; Fig. 6C), however the absolute change in OH between the simulation with and without halogen peaks in the tropical free troposphere. The lower OH concentration in our simulation prolongs the lifetimes of methane against tropospheric oxidation by OH by 16 % to 9.5 years, better matching the current best observational estimate of 11.2 ± 1.3 years [*Prather et al.*, 2012].

Bromine chemistry may also have implications for the atmospheric lifetime and deposition of mercury. The Br atom, which cycles photochemically with BrO, is thought

to be the the main atmospheric oxidant of Hg(0) [*Goodsite et al.*, 2004; *Holmes et al.*, 2006, 2010]. Using the Hg oxidation mechanism of *Holmes et al.* [2006] and the Br fields of our simulation A we estimate a global mean atmospheric lifetime of 6 months for Hg(0) against oxidation to Hg(II) by Br. This is consistent with observations of Hg(0) atmospheric gradients implying a lifetime of $0.5-2$ years against deposition [*Slemr et al.*, 1985], which would be longer than the lifetime of Hg(0) against oxidation if atmospheric Hg(II) reduction takes place [*Holmes et al.*, 2010]. A major difference between our results and those of *Holmes et al.* [2010] and *Parrella et al.* [2012] is that our simulated Br concentrations are much lower over the Southern Ocean due to suppression of Br_y release from sea salt, so that mercury deposition in that region is lower. Using the more recent *Dibble et al.* [2012] mechanism as implemented in GEOS-Chem by *Horowitz et al.* [manuscript in preparation, 2015] with our halogen fields (Br, BrO, Cl, and ClO), we find a global atmospheric lifetime of 3 months for Hg(0) against oxidation to Hg(II).

6. Conclusion

We used recent aircraft observations of BrO in the tropical and subtropical atmosphere, together with satellite observations, to improve our understanding of global tropospheric bromine chemistry and its implications. The observations point to higher background concentrations of BrO in the free troposphere than have been simulated by past models.

Sustaining the high levels of BrO seen in the observations requires rapid recycling of bromine radicals ($BrO_x \equiv$Br+BrO) from the pool of non-radical Br_y reservoirs. This can be achieved through multiphase chemistry in aerosols and clouds. We followed recommendations from IUPAC [*Ammann et al.*, 2013] by implementing into the GEOS-Chem global chemical transport model (CTM) an ensemble of multiphase halogen reactions including

oxidation of HBr/Br^- by HOBr, $ClNO_3$, and ozone in aerosols as well as liquid and ice clouds. This involved the addition of tropospheric chlorine chemistry in GEOS-Chem, enabling a broader examination of coupled Br–Cl chemistry. It also involved coupling of bromine chemistry to a dynamic simulation of sea salt aerosol (SSA) alkalinity since release of SSA bromide requires an acidified aerosol. The SSA-driven source of bromine radicals was not included in the standard simulation (A) but was examined in a sensitivity simulation (B).

Results from the updated GEOS-Chem simulation indicate a global mean tropospheric BrO concentration of about 1 ppt in the daytime. Most of this BrO is in the free troposphere where its main source is from oxidation and photolysis of marine biogenic bromoform ($CHBr_3$). Stratospheric input also contributes in the upper troposphere. The dominant bromine reservoirs are HOBr in the daytime and BrCl at night, reflecting the rapid recycling of HBr in cloud and sulfate aerosol. Debromination of SSA improves BrO observations in the marine boundary layer over the Western Pacific, but presents a challenge to reconcile model predictions with observations of low BrO in the marine boundary layer over the tropical Eastern Pacific.

Our simulated BrO concentrations are consistent with GOME-2 and OMI satellite column observations in the tropics and mid-latitudes, and corroborate cloud-slicing analysis and aircraft observations indicating that most tropospheric BrO is in the free troposphere. We find that the troposphere accounts for over half of the total (troposphere + stratosphere) BrO column in the subtropics. The model reproduces the increase of BrO with altitude in HCRERO aircraft observations over the subsiding Southeast Pacific.

Halogen (bromine-chlorine) chemistry as implemented in our simulation decreases the global burden of tropospheric ozone in GEOS-Chem by 14 % ($2-7$ ppb in the tropics and $6-10$ ppb at mid-latitudes). This reflects a decrease in chemical production of ozone by 10 % (due to halogen-driven NO_x loss) and a shortening of the ozone lifetime by 5.6 % (due to Br-catalyzed ozone loss). In most of the troposphere, halogen chemistry decreases NO_x levels through formation of halogen nitrates followed by hydrolysis to HNO_3. In polluted boundary layers, however, halogen chemistry increases NO_x levels by decreasing OH. Thus halogen chemistry decreases mean surface ozone concentrations in the US by only $2-6$ ppb, and increases the relative importance of regional pollution from domestic NO_x sources vs. transported background ozone. Halogen chemistry lowers global mean tropospheric OH concentrations by 11 %, driven by decreases in both ozone and NO_x. The resulting methane lifetime against oxidation by tropospheric OH in GEOS-Chem increases by 16 % to 9.5 years, improving the agreement with current best estimates. The global mean atmospheric lifetime of elemental mercury Hg(0) against oxidation to Hg(II) by Br atoms is 6 months, within the observational constraints. Alkaline SSA over the Southern Ocean implies that Br atom concentrations should be relatively low there, suppressing Hg(II) deposition.

Acknowledgments. JAS acknowledges support from The Danish Council for Independent Research | Natural Sciences. This work was supported by the NASA Atmospheric Composition Modeling and Analysis Program (grants to DJJ and QL). We acknowledge Eric Apel and the TORERO Science Team. The TORERO project is funded by the National Science Foundation (NSF) under Award AGS-1104104 (Principal Investigator: R.V.). The involvement of the NSF-sponsored Lower Atmospheric Observing Facilities,

421 managed and operated by the National Center for Atmospheric Research Earth Observ-
422 ing Laboratory, is acknowledged. S.W. is a recipient of the Fulbright Junior Research
423 Award. We acknowledge the CAST Science Team. We acknowledge C. Brenninkmei-
424 jer, A. Rauthe-Schoech, and the CARIBIC Science Team. We acknowledge E. Atlas, S.
425 Montzka, and the HIPPO Science Team. NOAA flask measurements onboard the HIPPO
426 missions were provided by S. Montzka, F. Moore, B. Miller, C. Sweeney, and J. Elkins, and
427 were supported in part by NOAA Climate Progam Office's AC4 program. GEOS-Chem
428 is available to the community through the standard GEOS-Chem repository www.geos-
429 chem.org. Model output from the simulations described above are available upon request
430 (schmidt@chem.ku.dk). Observational data from the TORERO campaign is available to
431 the community through http://www.eol.ucar.edu/node/4527.

References

432 Alexander, B., R. J. Park, D. J. Jacob, Q. B. Li, R. M. Yantosca, J. Savarino, C. C. W.
433 Lee, and T. M. H. (2005), Sulfate formation in sea-salt aerosols: Constraints from
434 oxygen isotopes, *J. Geophys. Res.*, *110*, D10,307, doi:10.1029/2004JD005659.
435 Alexander, B., D. J. Allman, H. M. Amos, T. D. Fairlie, J. Dachs, D. A. Hegg, and
436 R. S. Sletten (2012), Isotopic constraints on sulfate aerosol formation pathways in the
437 marine boundary layer of the subtropical northeast Atlantic Ocean, *J. Geophys. Res.*,
438 *117*, D06,304, doi:10.1029/2011JD016773.
439 Ammann, M., R. A. Cox, J. N. Crowley, M. E. Jenkin, A. Mellouki, M. J. Rossi, J. Troe,
440 and T. J. Wallington (2013), Evaluated kinetic and photochemical data for atmospheric
441 chemistry: Volume VI heterogeneous reactions with liquid substrates, *Atmos. Chem.*

Phys., *13*, 8045–8228, doi:10.5194/acp-13-8045-2013.

Amos, H. M., D. J. Jacob, C. D. Holmes, J. A. Fisher, Q. Wang, R. M. Yantosca, E. S. Corbitt, E. Galarneau, A. P. Rutter, M. S. Gustin, A. Steffen, J. J. Schauer, J. A. Graydon, V. L. S. Louis, R. W. Talbot, E. S. Edgerton, Y. Zhang, and E. M. Sunderland (2012), Gas-particle partitioning of atmospheric Hg(II) and its effect on global mercury deposition, *Atmos. Chem. Phys.*, *12*(1), 591–603, doi:10.5194/acp-12-591-2012.

Barrie, L. A., J. W. Bottenheim, R. C. Schnell, P. J. Crutzen, and R. A. Rasmussen (1988), Ozone destruction and photochemical-reactions at polar sunrise in the lower Arctic atmosphere, *Nature*, *334*, 138–141, doi:10.1038/334138a0

Beckwith, R. C., T. X. Wang, and D. W. Margerum (1996), Equilibrium and kinetics of bromine hydrolysis, *Inorganic Chemistry*, *35*(4), 995–1000, doi:10.1021/ic950909w.

Bogdan, A., M. J. Molina, K. Sassen, and M. Kulmala (2006), Formation of low-temperature cirrus from H_2SO_4/H_2O aerosol droplets, *J. Phys. Chem. A*, *110*(46), 12,541–12,542, doi:10.1021/jp065898e.

Bogdan, A., M. J. Molina, H. Tenhu, E. Mayer, and T. Loerting (2010), Formation of mixed-phase particles during the freezing of polar stratospheric ice clouds, *Nat. Chem.*, *2*, 197–201, doi:10.1038/nchem.540.

Breider, T. J., M. P. Chipperfield, N. A. D. Richards, K. S. Carslaw, G. W. Mann, and D. V. Spracklen (2010), Impact of BrO on dimethylsulfide in the remote marine boundary layer, *Geophys. Res. Lett.*, *37*, L02,807, doi:10.1029/2009GL040868.

Coburn, S., B. Dix, E. Edgerton, C. D. Holmes, D. Kinnison, Q. Liang, A. ter Schure, S. Y. Wang, and R. Volkamer (2016), Mercury oxidation from bromine chemistry in the free troposphere over the Southeastern US, *Atmos. Chem. Phys.*, *16*(6), 3743–3760,

doi:10.5194/acp-16-3743-2016.

Deiber, G., C. George, S. Le Calvé, F. Schweitzer, and P. Mirabel (2004), Uptake study of $ClONO_2$ and $BrONO_2$ by halide containing droplets, *Atmos. Chem. Phys.*, *4*(5), 1291–1299, doi:10.5194/acp-4-1291-2004.

Dibble, T. S., M. J. Zelie, and H. Mao (2012), Thermodynamics of reactions of ClHg and BrHg radicals with atmospherically abundant free radicals, *Atmos. Chem. Phys.*, *12*(21), 10,271–10,279, doi:10.5194/acp-12-10271-2012.

Dix, B., S. Baidar, J. F. Bresch, S. R. Hall, K. S. Schmidt, S. Wang, and R. Volkamer (2013), Detection of iodine monoxide in the tropical free troposphere, *Proc. Natl. Acad. Sci. USA*, *110*(6), 2035–2040, doi:10.1073/pnas.1212386110.

Eastham, S. D., D. K. Weisenstein, and S. R. H. Barrett (2014), Development and evaluation of the unified troposphericstratospheric chemistry extension (UCX) for the global chemistry-transport model GEOS-Chem, *Atmos. Environ.*, *89*, 52–63, doi:10.1016/j.atmosenv.2014.02.001.

Fernandez, R. P., R. J. Salawitch, D. E. Kinnison, J.-F. Lamarque, and A. Saiz-Lopez (2014), Bromine partitioning in the tropical tropopause layer: implications for stratospheric injection, *Atmospheric Chemistry and Physics*, *14*(24), 13,391–13,410, doi:10.5194/acp-14-13391-2014.

Fickert, S., J. W. Adams, and J. N. Crowley (1999), Activation of Br_2 and BrCl via uptake of HOBr onto aqueous salt solutions, *J. Geophys. Res.*, *104(D19)*, 23,719–23,727, doi:10.1029/1999JD900359.

Froyd, K. D., D. M. Murphy, T. J. Sanford, D. S. Thomson, J. C. Wilson, L. Pfister, and L. Lait (2009), Aerosol composition of the tropical upper troposphere, *Atmospheric*

Chemistry and Physics, *9*(13), 4363–4385, doi:10.5194/acp-9-4363-2009.

Gomez Martin, J. C., A. S. Mahajan, T. D. Hay, C. Prados-Roman, C. Ordonez, S. M. MacDonald, J. M. Plane, M. Sorribas, M. Gil, J. F. Paredes Mora, M. V. Agama Reyes, D. E. Oram, E. Leedham, and A. Saiz-Lopez (2013), Iodine chemistry in the eastern Pacific marine boundary layer, *J. Geophys. Res.*, *118*(2), 887–904, doi:10.1002/jgrd.50132.

Goodsite, M. E., J. M. C. Plane, and H. Skov (2004), A theoretical study of the oxidation of Hg^0 to HgBr2 in the troposphere, *Environmental Science & Technology*, *38*(6), 1772–1776, doi:10.1021/es034680s.

Gratz, L. E., J. L. Ambrose, D. A. Jaffe, V. Shah, L. Jaegle, J. Stutz, J. Festa, M. Spolaor, C. Tsai, N. E. Selin, S. Song, X. Zhou, A. J. Weinheimer, D. J. Knapp, D. D. Montzka, F. M. Flocke, T. L. Campos, E. Apel, R. Hornbrook, N. J. Blake, S. Hall, G. S. Tyndall, M. Reeves, D. Stechman, and M. Stell (2015), Oxidation of mercury by bromine in the subtropical Pacific free troposphere, *Geophys. Res. Lett.*, doi:10.1002/2015GL066645, 2015GL066645.

Holmes, C. D., D. J. Jacob, and X. Yang (2006), Global lifetime of elemental mercury against oxidation by atomic bromine in the free troposphere, *Geophys. Res. Lett.*, *33*(20), doi:10.1029/2006GL027176, l20808.

Holmes, C. D., D. J. Jacob, E. S. Corbitt, J. Mao, X. Yang, R. Talbot, and F. Slemr (2010), Global atmospheric model for mercury including oxidation by bromine atoms, *Atmos. Chem. Phys.*, *10*, 12,037–12,057, doi:10.5194/acp-10-12037-2010.

Hossaini, R., M. P. Chipperfield, B. M. Monge-Sanz, N. A. D. Richards, E. Atlas, and D. R. Blake (2010), Bromoform and dibromomethane in the tropics: a 3-d model study of chemistry and transport, *Atmospheric Chemistry and Physics*, *10*(2), 719–735, doi:

511 10.5194/acp-10-719-2010.

512 Jaegle, L., P. K. Quinn, T. S. Bates, B. Alexander, and J.-T. Lin (2011), Global distribu-
513 tion of sea salt aerosols: new constraints from in situ and remote sensing observations,
514 *Atmos. Chem. Phys.*, *11*, 3137–3157, doi:10.5194/acp-11-3137-2011.

515 Leser, H., C. Hönninger, and U. Platt (2003), MAX-DOAS measurements of BrO and NO_2
516 in the marine boundary layer, *Geophys. Res. Lett.*, *30*, 1537, doi:10.1029/2002GL015811.

517 Lewis, E. R., and S. E. Schwartz (2004), Sea salt aerosol production: Mechanisms, meth-
518 ods, measurements and models - a critical review, american geophysical union, wash-
519 ington, d. c., doi:10.1002/9781118666050.fmatter.

520 Liang, L., and P. C. Singer (2003), Factors influencing the formation and relative distribu-
521 tion of haloacetic acids and trihalomethanes in drinking water, *Environmental Science*
522 *& Technology*, *37*(13), 2920–2928.

523 Liang, Q., R. S. Stolarski, S. R. Kawa, J. E. Nielsen, A. R. Douglass, J. M. Rodriguez,
524 D. R. Blake, E. L. Atlas, and L. E. Ott (2010), Finding the missing stratospheric Br_y:
525 a global modeling study of $CHBr_3$ and $CH2Br_2$, *Atmos. Chem. Phys.*, *10*, 2269–2286,
526 doi:10.5194/acp-10-2269-2010.

527 Liang, Q., E. Atlas, D. Blake, M. Dorf, K. Pfeilsticker, and S. Schauffler (2014), Convective
528 transport of very short lived bromocarbons to the stratosphere, *Atmospheric Chemistry*
529 *and Physics*, *14*(11), 5781–5792, doi:10.5194/acp-14-5781-2014.

530 Long, M. S., W. C. Keene, R. C. Easter, R. Sander, X. Liu, A. Kerkweg, and D. Erickson
531 (2014), Sensitivity of tropospheric chemical composition to halogen-radical chemistry
532 using a fully coupled size-resolved multiphase chemistryglobal climate system: halo-
533 gen distributions, aerosol composition, and sensitivity of climate-relevant gases, *Atmos.*

Chem. Phys., *14*, 3397–3425, doi:10.5194/acp-14-3397-2014.

Martin, M., D. Pöhler, K. Seitz, R. Sinreich, and U. Platt (2009), BrO measurements over the Eastern North-Atlantic, *Atmos. Chem. Phys.*, *9*, 9545–9554, doi:10.5194/acp-9-9545-2009.

Montzka, S. A., S. Reimann, A. Engel, K. Krger, S. O'Doherty, W. T. Sturges, D. R. Blake, M. Dorf, P. Fraser, L. Froidevaux, K. W. Jucks, K. Kreher, M. J. Kurylo, A. Mellouki, J. Miller, O.-J. Nielsen, V. L. Orkin, R. G. Prinn, R. Rhew, M. L. Santee, A. Stohl, and D. Verdonik (2010), Ozone-Depleting Substances (ODSs) and related chemicals, chapter 1 in scientific assessment of ozone depletion: 2010, Global Ozone Research and Monitoring Project-Report No. 52, 516 pp., World Meteorological Organization, Geneva, Switzerland.

Murray, L. T., D. J. Jacob, J. A. Logan, R. C. Hudman, and W. J. Koshak (2012), Optimized regional and interannual variability of lightning in a global chemical transport model constrained by LIS/OTD satellite data, *J. Geophys. Res.*, *117*, D20,307, doi:10.1029/2012JD017934.

Nilsson, E. J. K., L. M. T. Joelsson, J. Heimdal, M. S. Johnson, and O. J. Nielsen (2013), Re-evaluation of the reaction rate coefficient of CH_3Br+OH with implications for the atmospheric budget of methyl bromide, *Atmos. Environ.*, *80*, 70–74, doi:10.1016/j.atmosenv.2013.07.046.

Ordóñez, C., J.-F. Lamarque, S. Tilmes, D. E. Kinnison, E. L. Atlas, D. R. Blake, G. Sousa Santos, G. Brasseur, and A. Saiz-Lopez (2012), Bromine and iodine chemistry in a global chemistry-climate model: description and evaluation of very short-lived oceanic sources, *Atmos. Chem. Phys.*, *12*, 1423–1447, doi:10.5194/acp-12-1423-2012.

Park, R. J., D. J. Jacob, B. D. Field, R. M. Yantosca, and M. Chin (2004), Natural and transboundary pollution influences on sulfate-nitrate-ammonium aerosols in the United States: Implications for policy, *J. Geophys. Res.*, *109*(D15), D15,204, doi:10.1029/2003JD004473.

Parrella, J. P., D. J. Jacob, Q. Liang, Y. Zhang, L. J. Mickley, B. Miller, M. J. Evans, X. Yang, J. A. Pyle, N. Theys, and M. Van Roozendael (2012), Tropospheric bromine chemistry: implications for present and pre-industrial ozone and mercury, *Atmos. Chem. Phys.*, *12*, 6723–6740, doi:10.5194/acp-12-6723-2012.

Paulot, F., D. J. Jacob, M. T. Johnson, T. G. Bell, A. R. Baker, W. C. Keene, I. D. Lima, S. C. Doney, and C. A. Stock (2015), Global oceanic emission of ammonia: Constraints from seawater and atmospheric observations, *Global Biogeochemical Cycles*, doi:10.1002/2015GB005106, 2015GB005106.

Platt, U., and G. Hönninger (2003), The role of halogen species in the troposphere, *Chemosphere*, *52*(2), 325–338, doi:http://dx.doi.org/10.1016/S0045-6535(03)00216-9.

Prados-Roman, C., A. Butz, T. Deutschmann, M. Dorf, L. Kritten, A. Minikin, U. Platt, H. Schlager, H. Sihler, N. Theys, M. Van Roozendael, T. Wagner, and K. Pfeilsticker (2011), Airborne DOAS limb measurements of tropospheric trace gas profiles: case studies on the profile retrieval of O_4 and BrO, *Atmos. Meas. Tech.*, *4*(6), 1241–1260, doi:10.5194/amt-4-1241-2011.

Prather, M. J., C. D. Holmes, and J. Hsu (2012), Reactive greenhouse gas scenarios: Systematic exploration of uncertainties and the role of atmospheric chemistry, *Geophysical Research Letters*, *39*(9), L09,803, doi:10.1029/2012GL051440.

Pye, H. O. T., H. Liao, S. Wu, L. J. Mickley, D. J. Jacob, D. K. Henze, and J. H. Seinfeld (2009), Effect of changes in climate and emissions on future sulfate-nitrate-ammonium aerosol levels in the United States, *J. Geophys. Res.*, *114*(D1), D01,205, doi:10.1029/2008JD010701.

Read, K. A., A. S. Mahajan, L. J. Carpenter, M. J. Evans, B. V. E. Faria, D. E. Heard, J. R. Hopkins, J. D. Lee, S. J. Moller, A. C. Lewis, L. Mendes, J. B. McQuaid, H. Oetjen, A. Saiz-Lopez, M. J. Pilling, and J. M. C. Plane (2008), Extensive halogen-mediated ozone destruction over the tropical Atlantic Ocean, *Nature*, *453*, 1232–1235, doi:10.1038/nature07035.

Saiz-Lopez, A., J. M. C. Plane, and J. A. Shillito (2004), Bromine oxide in the mid-latitude marine boundary layer, *Geophys. Res. Lett.*, *31*, L03,111, doi:10.1029/2003GL018956.

Saiz-Lopez, A., J.-F. Lamarque, D. E. Kinnison, S. Tilmes, C. Ordóñez, J. J. Orlando, A. J. Conley, J. M. C. Plane, A. S. Mahajan, G. Sousa Santos, E. L. Atlas, D. R. Blake, S. P. Sander, S. Schauffler, A. M. Thompson, and G. Brasseur (2012), Estimating the climate significance of halogen-driven ozone loss in the tropical marine troposphere, *Atmos. Chem. Phys.*, *12*, 3939–3949, doi:10.5194/acp-12-3939-2012.

Sander, R., W. C. Keene, A. A. P. Pszenny, R. Arimoto, G. P. Ayers, E. Baboukas, J. M. Cainey, P. J. Crutzen, R. A. Duce, G. Hnninger, B. J. Huebert, W. Maenhaut, N. Mihalopoulos, V. C. Turekian, and R. Van Dingenen (2003), Inorganic bromine in the marine boundary layer: a critical review, *Atmos. Chem. Phys.*, *3*, 1301–1336, doi:10.5194/acp-3-1301-2003.

Sherwen, T., M. J. Evans, L. J. Carpenter, S. J. Andrews, R. T. Lidster, B. Dix, T. K. Koenig, R. Volkamer, A. Saiz-Lopez, C. Prados-Roman, A. S. Mahajan, and C. Ordóñez

(2016), Iodine's impact on tropospheric oxidants: a global model study in GEOS-Chem, *Atmospheric Chemistry and Physics*, *16*(2),1161–1186, doi:10.5194/acp-16-1161-2016.

Simpson, W. R., R. von Glasow, K. Riedel, P. Anderson, P. Ariya, J. Bottenheim, J. Burrows, L. J. Carpenter, U. Frieß, M. E. Goodsite, D. Heard, M. Hutterli, H.-W. Jacobi, L. Kaleschke, B. Neff, J. Plane, U. Platt, A. Richter, H. Roscoe, R. Sander, P. Shepson, J. Sodeau, A. Steffen, T. Wagner, and E. Wolff (2007), Halogens and their role in polar boundary-layer ozone depletion, *Atmos. Chem. Phys.*, *7*(16), 4375–4418, doi:10.5194/acp-7-4375-2007.

Simpson, W. R., S. S. Brown, A. Saiz-Lopez, J. A. Thornton, and R. von Glasow (2015), Tropospheric halogen chemistry: Sources, cycling, and impacts, *Chemical Reviews*, *115*(10), 4035–4062, doi:10.1021/cr5006638.

Sinnhuber, B.-M., A. Rozanov, N. Sheode, O. T. Afe, A. Richter, M. Sinnhuber, F. Wittrock, J. P. Burrows, G. P. Stiller, T. von Clarmann, and A. Linden (2005), Global observations of stratospheric bromine monoxide from sciamachy, *Geophysical Research Letters*, *32*(20), n/a–n/a, doi:10.1029/2005GL023839, l20810.

Slemr, F., G. Schuster, and W. Seiler (1985), Distribution, speciation, and budget of atmospheric mercury, *Journal of Atmospheric Chemistry*, *3*(4), 407–434, doi:10.1007/BF00053870.

Theys, N., M. Van Roozendael, F. Hendrick, X. Yang, I. De Smedt, A. Richter, M. Begoin, Q. Errera, P. V. Johnston, K. Kreher, , and M. De Mazire (2011), Global observations of tropospheric BrO columns using GOME-2 satellite data, *Atmos. Chem. Phys.*, *11*, 1791–1811, doi:10.5194/acp-11-1791-2011.

Thornton, J. A., J. P. Kercher, T. P. Riedel, N. L. Wagner, J. Cozic, J. S. Holloway, W. P. Dubé, G. M. Wolfe, P. K. Quinn, A. M. Middlebrook, et al. (2010), A large atomic chlorine source inferred from mid-continental reactive nitrogen chemistry, *Nature*, *464*(7286), 271–274.

Volkamer, R., S. Baidar, T. L. Campos, S. Coburn, J. P. DiGangi, B. Dix, T. K. Koenig, I. Ortega, B. R. Pierce, M. Reeves, R. Sinreich, S. Wang, M. A. Zondlo, and P. A. Romashkin (2015), NO_2, H_2O, O_2-O_2 and aerosol extinction profiles in the tropics: Comparison with aircraft-/ship-based in situ and lidar measurements, *Atmos. Meas. Tech.*, *8*(1), 2121–2148, doi:10.5194/amt-8-2121-2015.

von Glasow, R., R. von Kuhlmann, M. G. Lawrence, U. Platt, and P. J. Crutzen (2004), Impact of reactive bromine chemistry in the troposphere, *Atmos. Chem. Phys.*, *4*(11/12), 2481–2497, doi:10.5194/acp-4-2481-2004.

Wang, Q., D. J. Jacob, J. A. Fisher, J. Mao, E. M. Leibensperger, C. C. Carouge, P. Le Sager, Y. Kondo, J. L. Jimenez, M. J. Cubison, and S. J. Doherty (2011), Sources of carbonaceous aerosols and deposited black carbon in the arctic in winter-spring: implications for radiative forcing, *Atmos. Chem. Phys.*, *11*(23), 12,453–12,473, doi:10.5194/acp-11-12453-2011.

Wang, S., J. A. Schmidt, S. Baidar, S. Coburn, B. Dix, T. K. Koenig, E. Apel, D. Bowdalo, T. L. Campos, E. Eloranta, M. J. Evans, J. P. DiGangi, M. A. Zondlo, R.-S. Gao, J. A. Haggerty, S. R. Hall, R. S. Hornbrook, D. Jacob, B. Morley, B. Pierce, M. Reeves, P. Romashkin, A. ter Schure, and R. Volkamer (2015), Active and widespread halogen chemistry in the tropical and subtropical free troposphere, *Proc. Natl. Acad. Sci. USA*, doi:10.1073/pnas.1505142112.

Wang, Y., D. J. Jacob, and J. A. Logan (1998), Global simulation of tropospheric O_3-NO_x-hydrocarbon chemistry: 1. Model formulation, *J. Geophys. Res.*, *103*(D9), 10,713–10,725, doi:10.1029/98JD00158.

Warwick, N. J., J. A. Pyle, G. D. Carver, X. Yang, N. H. Savage, F. M. O'Connor, and R. A. Cox (2006), Global modeling of biogenic bromocarbons, *J. Geophys. Res.*, *111*(D24), doi:10.1029/2006JD007264.

Wesely, M. (1989), Parameterization of surface resistances to gaseous dry deposition in regional-scale numerical models, *Atmos. Environ.*, *23*(6), 1293 – 1304, doi: http://dx.doi.org/10.1016/0004-6981(89)90153-4.

Wisher, A., D. E. Oram, J. C. Laube, G. P. Mills, P. van Velthoven, A. Zahn, and C. A. M. Brenninkmeijer (2014), Very short-lived bromomethanes measured by the CARIBIC observatory over the North Atlantic, Africa and Southeast Asia during 2009–2013, *Atmos. Chem. Phys.*, *14*(7), 3557–3570, doi:10.5194/acp-14-3557-2014.

Wofsy, S. C., B. C. Daube, R. Jimenez, E. Kort, J. V. Pittman, S. Park, R. Commane, B. Xiang, G. Santoni, D. Jacob, J. Fisher, C. Pickett-Heaps, H. Wang, K. Wecht, Q.-Q. Wang, B. B. Stephens, S. Shertz, A. S. Watt, P. Romashkin, T. Campos, J. Haggerty, W. A. Cooper, D. Rogers, S. Beaton, R. Hendershot, J. W. Elkins, D. W. Fahey, R. S. Gao, F. Moore, S. A. Montzka, J. P. Schwarz, A. E. Perring, D. Hurst, B. R. Miller, C. Sweeney, S. Oltmans, D. Nance, E. Hintsa, G. Dutton, L. A. Watts, J. R. Spackman, K. H. Rosenlof, E. A. Ray, B. Hall, M. A. Zondlo, K. R. Diao, M., J. Bent, E. L. Atlas, R. Lueb, and M. J. Mahoney (2012a), HIPPO Combined Discrete Flask and GC Sample GHG, Halo-, Hydrocarbon Data (R_20121129), *Carbon Dioxide Information Analysis Center, Oak Ridge National Laboratory, Oak Ridge, Tennessee, U.S.A.*, doi:

http://dx.doi.org/10.3334/CDIAC/hippo_012.

Wofsy, S. C., B. C. Daube, R. Jimenez, E. Kort, J. V. Pittman, S. Park, R. Commane, B. Xiang, G. Santoni, D. Jacob, J. Fisher, C. Pickett-Heaps, H. Wang, K. Wecht, Q.-Q. Wang, B. B. Stephens, S. Shertz, A. S. Watt, P. Romashkin, T. Campos, J. Haggerty, W. A. Cooper, D. Rogers, S. Beaton, R. Hendershot, J. W. Elkins, D. W. Fahey, R. S. Gao, F. Moore, S. A. Montzka, J. P. Schwarz, A. E. Perring, D. Hurst, B. R. Miller, C. Sweeney, S. Oltmans, D. Nance, E. Hintsa, G. Dutton, L. A. Watts, J. R. Spackman, K. H. Rosenlof, E. A. Ray, B. Hall, M. A. Zondlo, K. R. Diao, M., J. Bent, E. J. Atlas, R. Lueb, and M. J. Mahoney (2012b), HIPPO NOAA Flask Sample GHG, Halocarbon, and Hydrocarbon Data (R_20121129), *Carbon Dioxide Information Analysis Center, Oak Ridge National Laboratory, Oak Ridge, Tennessee, U.S.A.*, doi: http://dx.doi.org/10.3334/CDIAC/hippo_013.

Wu, S., L. J. Mickley, D. J. Jacob, J. A. Logan, R. M. Yantosca, and D. Rind (2007), Why are there large differences between models in global budgets of tropospheric ozone?, *J. Geophys. Res.*, *112*, D05,302, doi:10.1029/2006JD007801.

Yang, X., R. A. Cox, N. J. Warwick, J. A. Pyle, G. D. Carver, F. M. O'Connor, and N. H. Savage (2005), Tropospheric bromine chemistry and its impacts on ozone: A model study, *J. Geophys. Res.*, *110*, D23,311, doi:10.1029/2005JD006244.

Table 1. Global sources of reactive inorganic halogens to the troposphere.

	Br_y / $Gg\,Br\,a^{-1}$	Cl_y / $Gg\,Cl\,a^{-1}$
Sea salt[a]	(1620)	(6050)
Organohalogens[b]		
CH_3X	91	2350
CH_2X_2	55	483
CHX_3	404	262
Stratosphere	49	407

[a] Release of inorganic bromine and chlorine from sea salt as included in simulation B (see text).

[b] X = Br or Cl.

Table 2. Reactive uptake coefficients for halogen multiphase hydrolysis.[a]

Reaction	Reactive uptake coefficient
$BrNO_3 \xrightarrow{H_2O} HOBr + HNO_3$	$\gamma' = (1/\Gamma_b + 1/\alpha_b)^{-1}$
	$\Gamma_b = 0.03$; $\alpha_b = 0.063$
$ClNO_3 \xrightarrow{H_2O} HOCl + HNO_3$	$\gamma' = (1/\Gamma_b + 1/\alpha_b)^{-1}$
	$\Gamma_b = 0.03$; $\alpha_b = 0.11$

[a] Parameters from *Ammann et al.* [2013] unless otherwise stated. γ' is defined implicitly from Eq. 2.2, and is equal to the reactive uptake coefficient (γ) when gas phase diffusion is not limiting. α_b and Γ_b are the mass accommodation coefficient and the bulk reaction coefficient, respectively. The previous GEOS-Chem study [*Parrella et al.*, 2012] included $BrNO_3$ hydrolysis with $\gamma' = 0.3$ for sea salt and liquid cloud droplets and 0.8 for sulfate aerosol. Our Γ_b is estimated from observed γ' reported by *Deiber et al.* [2004].

Table 3. Reactive uptake coefficients for multiphase oxidation of halide ions.[a]

Reaction	Reactive uptake coefficient
$HOBr + Br^- + H^+ \longrightarrow Br_2 + H_2O$	$\gamma' = (1/\Gamma_b + 1/\alpha_b)^{-1}$
	$\Gamma_b = 4\,H_{\mathrm{HOBr}}\,RT\,l_r\,k_{\mathrm{bulk}}\,[\mathrm{Br^-}]\,[\mathrm{H^+}]\,\mathrm{f(r,l_r)/c}$
	$l_r = \sqrt{D_l/(k_{\mathrm{bulk}}\,[\mathrm{Br^-}]\,[\mathrm{H^+}])};\quad \alpha_b = 0.6$
	$k_{\mathrm{bulk}} = 1.6\,\times\,10^{10}\,\mathrm{M^{-2}s^{-1}};\ D_l = 1.4\,\times\,10^{-5}\,\mathrm{cm^2\,s^{-1}}$
$HOBr + Cl^- + H^+ \longrightarrow BrCl + H_2O$	$\gamma' = (1/\Gamma_b + 1/\alpha_b)^{-1}$
	$\Gamma_b = 4\,H_{\mathrm{HOBr}}\,RT\,l_r\,k_{\mathrm{bulk}}\,[\mathrm{Cl^-}]\,[\mathrm{H^+}]\,\mathrm{f(r,l_r)/c}$
	$l_r = \sqrt{D_l/(k_{\mathrm{bulk}}\,[\mathrm{Cl^-}]\,[\mathrm{H^+}])};\quad \alpha_b = 0.6$
	$k_{\mathrm{bulk}} = 5.9\,\times\,10^{9}\,\mathrm{M^{-2}s^{-1}};\ D_l = 1.4\,\times\,10^{-5}\,\mathrm{cm^2\,s^{-1}}$
$ClNO_3 + Br^- \longrightarrow BrCl + NO_3^-$	$\gamma' = (1/\Gamma_b + 1/\alpha_b)^{-1}$
	$\Gamma_b = 4\,W\,RT\,\sqrt{[\mathrm{Br^-}]\,\mathrm{D_l}}/c;\quad \alpha_b = 0.108$
	$D_l = 5.0\,\times\,10^{-6}\,\mathrm{cm^2\,s^{-1}};\ W = 10^6\,\sqrt{\mathrm{M\,s}}\,\mathrm{bar}^{-1}$
$O_3 + Br^- \xrightarrow{H_2O} HOBr + OH^- + O_2$	$\gamma' = \Gamma_b + \Gamma_s$
	$\Gamma_b = 4\,H_{\mathrm{O3}}\,RT\,l_r\,k_{\mathrm{bulk}}\,[\mathrm{Br^-}]\,\mathrm{f(r,l_r)/c}$
	$l_r = \sqrt{D_l/(k_{\mathrm{bulk}}\,[\mathrm{Br^-}])};\quad D_l = 8.9\,\times\,10^{-6}\,\mathrm{cm^2\,s^{-1}}$
	$k_{\mathrm{bulk}} = 6.3\times10^{8}\mathrm{M^{-1}s^{-1}}\,\exp(-4450\mathrm{K/T})$
	$\Gamma_s = (4\,k_s\,[\mathrm{Br^-(surf)}]\,\mathrm{K_{LangC}\,N_{max}})/(\mathrm{c_{avg}}\,(1+\mathrm{K_{LangC}}\,[\mathrm{O_3(g)}]))$
	$[\mathrm{Br^-(surf)}] = \min(3.41\times10^{14}\,\mathrm{cm^{-2}M^{-1}}\,[\mathrm{Br^-}], \mathrm{N_{max}})$
	$k_s = 10^{-16}\,\mathrm{cm^2s^{-1}};\ K_{\mathrm{LangC}} = 10^{-13}\mathrm{cm^3};\ N_{\mathrm{max}} = 3.0\times10^{14}\mathrm{cm^{-2}}$

[a] Parameters from *Ammann et al.* [2013] unless otherwise stated. The previous GEOS-Chem study [*Parrella et al.*, 2012] included multiphase HOBr+HBr with $\gamma' = 0.2$ for sea salt and sulfate aerosol, and 0.1 for ice cloud droplets. k_{bulk} for HOBr+Br^- is taken from *Beckwith et al.* [1996]. For sea salt aerosol HOBr+Cl^- is assumed to be limited by mass accommodation or gas phase diffusion kinetics.

[trim = 0mm 15mm 0mm 0mm, clip, width=8.0cm]fig_jgr/2015jaX − p01a.eps

[trim = 0mm 0mm 0mm 0mm, clip, width=7.5cm]fig_jgr/2015jaX − p01b.eps

Figure 1. Global model budget and speciation of reactive tropospheric inorganic bromine (Br_y) for the simulation not including dehalogenation of sea salt aerosol (simulation A). Upper panel: Global annual mean inventory and cycling of Br_y species in the troposphere. Rates are in $Gg\,Br\,a^{-1}$, inventories are in $Gg\,Br$, and numbers in brackets are mean mixing ratios (ppt). Green arrows represent multiphase reactions. Arrow thickness scales with rate. Read 1.2(4) as 1.2×10^4. Daytime concentrations of BrO and Br are about twice the indicated values because nighttime concentrations are near zero (this approximation is not valid at high latitudes during winter and summer). Lower panel: Vertical profile of Br_y speciation during daytime (7:00-19:00) and nighttime (19:00-7:00) in the tropics. Values are annual mean mixing ratios in the $22°S - 22°N$ latitude range. The overall envelope gives total Br_y. The orange and dark blue slivers denote $BrNO_2$ and Br_2, respectively. The dashed line shows total Br_y from the simulation including SSA dehalogenation (simulation B).

[trim = 0mm 0mm 0mm 0mm, clip, width=8.5cm]fig_jgr/2015jaX − p02.eps

Figure 2. Simulated annual mean global distributions of tropospheric Br_y and BrO. Multiply BrO concentrations by a factor of 2 for daytime values (this approximation is not valid at high latitudes during winter and summer). Top panels: mean tropospheric mixing ratios. Bottom panels: zonal mean mixing ratios as a function of altitude and latitude. The tropopause is shown as dashed line. Results are for the simulation not including dehalogenation of SSA (simulation A).

[trim = 0mm 0mm 0mm 0mm, clip, width=8.5cm]fig$_j$gr/2015jaX − p03.eps

Figure 3. Seasonal variation of zonal mean tropospheric BrO columns in different latitudinal bands. 2007 observations from the GOME-2 satellite instrument [*Theys et al.*, 2011] are compared to GEOS-Chem values (simulation A) at the GOME-2 local overpass time (9:00 – 10:00). Columns obtained from the simulation including SSA dehalogenation are shown in cyan.

[trim = 0mm 0mm 0mm 0mm, clip, width=8.5cm]fig$_j$gr/2015jaX − p04.eps

Figure 4. Global distribution of the total annual mean BrO column including the troposphere and stratosphere. 2007 observations from the OMI satellite instrument (http://disc.sci.gsfc.nasa.gov/Aura/data-holdings/OMI/ombro_v003.shtml) are compared to tropospheric GEOS-Chem values (simulation A) for the OMI overpass time (13:00 – 14:00 local time) together with stratospheric values from GEOSCCM used as upper boundary condition for GEOS-Chem [*Liang et al.*, 2010]. The left panel separates the contributions from the troposphere and stratosphere to the total GEOS-Chem column.

[trim = 0mm 0mm 0mm 0mm, clip, width=8.5cm]fig$_j gr/2015jaX - p05.eps$

Figure 5. Mean vertical profiles of BrO concentration over the Southeast Pacific. Daytime aircraft observations from the TORERO campaign (January-February 2012; black cross) are compared to GEOS-Chem values (simulation A) sampled along the 17 flight tracks (red square). Also shown are results from model sensitivity simulations including SSA dehalogenation (simulation B; cyan triangle), without the aqueous phase O_3+Br^- reaction (green asterisk), and without multiphase halogen chemistry (gas-phase chemistry only; blue circle). The observed BrO in the MBL was below the instrument detection limit of about 0.5 ppt. The right panel shows the TORERO flight tracks superimposed on the model distribution of daytime tropospheric mean BrO mixing ratios for the flight period.

Table 4. Global tropospheric ozone budgets in GEOS-Chem (simulation A).[a]

	This study	No halogen
Sources ($Tg\,a^{-1}$)		
Chemistry	4964	5513
Stratosphere	515	510
Sinks ($Tg\,a^{-1}$)		
Chemistry	4500	4926
Deposition	979	1097
Burden (Tg)	329	383
Lifetime (days)	21.9	23.2

[a] The ozone budget is defined that of odd oxygen (see definition of O_x in text). The burden, production and loss rates are given in O_3 equivalent masses. Non-ozone O_x contribute less than 1 % of the burden.

[trim = 0mm 0mm 0mm 0mm, clip, width=8.5cm]fig$_j$gr/2015jaX − p07.eps

Figure 6. Effect of halogen chemistry in GEOS-Chem on the global annual NO_x levels, ozone production, OH levels, and methane loss. The effects are given as $((X)_{\mathrm{nohal}} - (X)_{\mathrm{GC}})/(X)_{\mathrm{nohal}}$, where $(X)_{\mathrm{nohal}}$ is concentration of X from the simulation without halogen chemistry and $(X)_{\mathrm{GC}}$ is from our GEOS-Chem reference simulation without SSA dehalogenation (simulation A). Panel A: color contours show relative change in NO_x. Black contours show GEOS-Chem NO_x mixing ratio (ppt). Panel B: color contours show relative change in chemical ozone production. Black contours show GEOS-Chem ozone production rates ($cm^{-3}s^{-1}$), read 5.5 as $10^{5.5}$. Panel C: color contours show relative change in OH. Black contours show GEOS-Chem OH concentration (cm^{-3}), read 6 as 10^6. Panel D: colour contours show relative change in methane loss rate. Black contours show GEOS-Chem methane loss rate (a^{-1}).

[trim = 0mm 0mm 0mm 0mm, clip, width=8.5cm]fig$_j$gr/2015jaX − p08a.eps

[trim = 0mm 25mm 0mm 0mm, clip, width=8.5cm]fig$_j$gr/2015jaX − p08b.eps

Figure 7. Effect of halogen chemistry on the global annual tropospheric ozone budget. The ozone budget is defined that of odd oxygen ($O_x \equiv O_3 + O + NO_2 + 2NO_3$ + peroxyacylnitrates + HNO_3 + HNO_4 + $3N_2O_5$ + XO + HOX + XNO_2 + $2XNO_3$ + Cl_2O_2 + 2OClO) to account for rapid cycling between O_x species. Upper panel: Relative contributions of different processes to O_x loss in the tropics (22°S to 22°N). Lower panel: Pathways for bromine-catalyzed ozone loss. Rates are in Gg Br a^{-1} (Global annual average).

[trim = 0mm 0mm 0mm 0mm, clip, width=8.5cm]fig$_j gr/2015jaX-p09.eps$

Figure 8. Effect of halogen chemistry on global tropospheric ozone concentrations. Values are annual mean differences between GEOS-Chem simulations not including vs. including halogen chemistry: Δozone is ozone from simulation with no halogen chemistry minus ozone from simulation A. Top panel: zonal mean difference. Middle panel: difference in tropospheric mean. Bottom panel: difference in surface concentration.

[trim = 0mm 0mm 0mm 0mm, clip, width=8.5cm]fig$_j gr/2015jaX-p10.eps$

Figure 9. Annual average vertical profile from ozonesonde observations for 5 zonal bands compared to model ozone from the current simulation and a simulation with no halogen chemistry. N_s and N_p are the number of sites and profiles, respectively, included in the averaging. The location of the sites is giving the supporting information.

[trim = 0mm 0mm 0mm 0mm, clip, width=8.5cm]fig$_j gr/2015jaX-p11.eps$

Figure 10. The global annual average GEOS-Chem budget of HO_x (OH and HO_2) simulated with (simulation A) and without halogen chemistry.

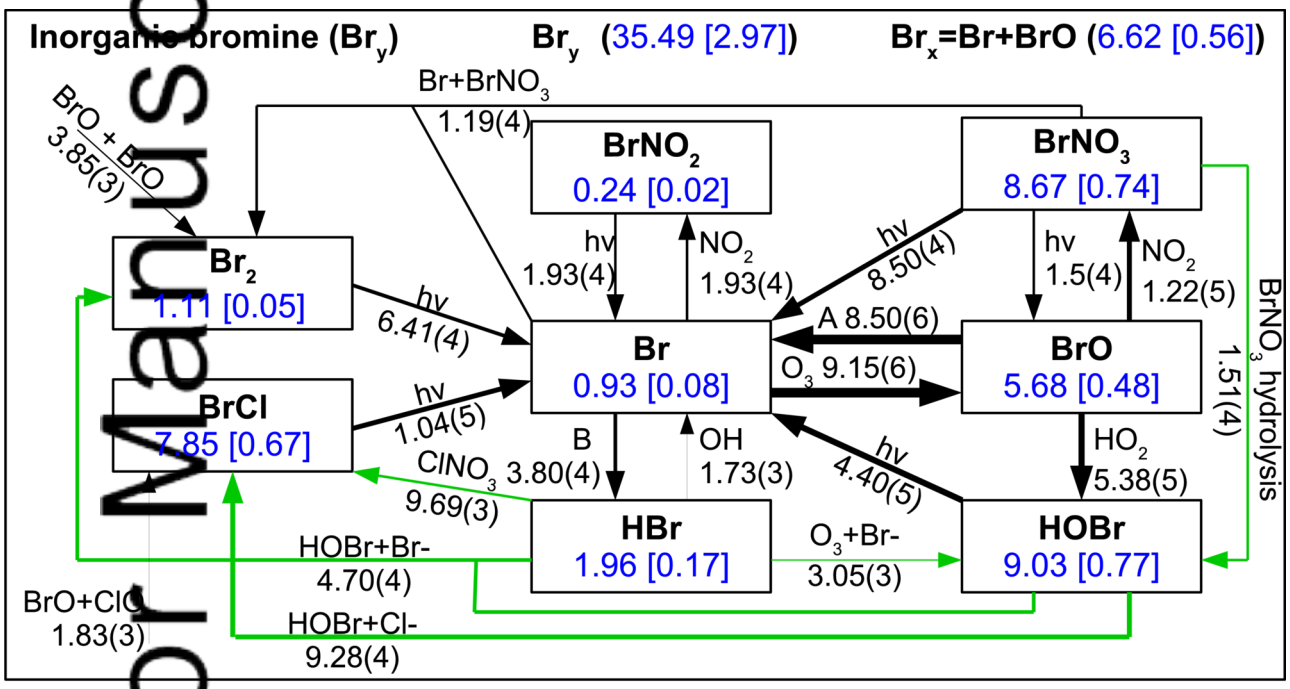

A = 80% (BrO + hv) + 19% (BrO + NO) + 1% (BrO + OH/BrO/ClO)

B = 73% (Br + CH_2O) + 17% (Br + CH_3CHO) + 10% (Br + HO_2)

2015jd024229-f01-z-.eps

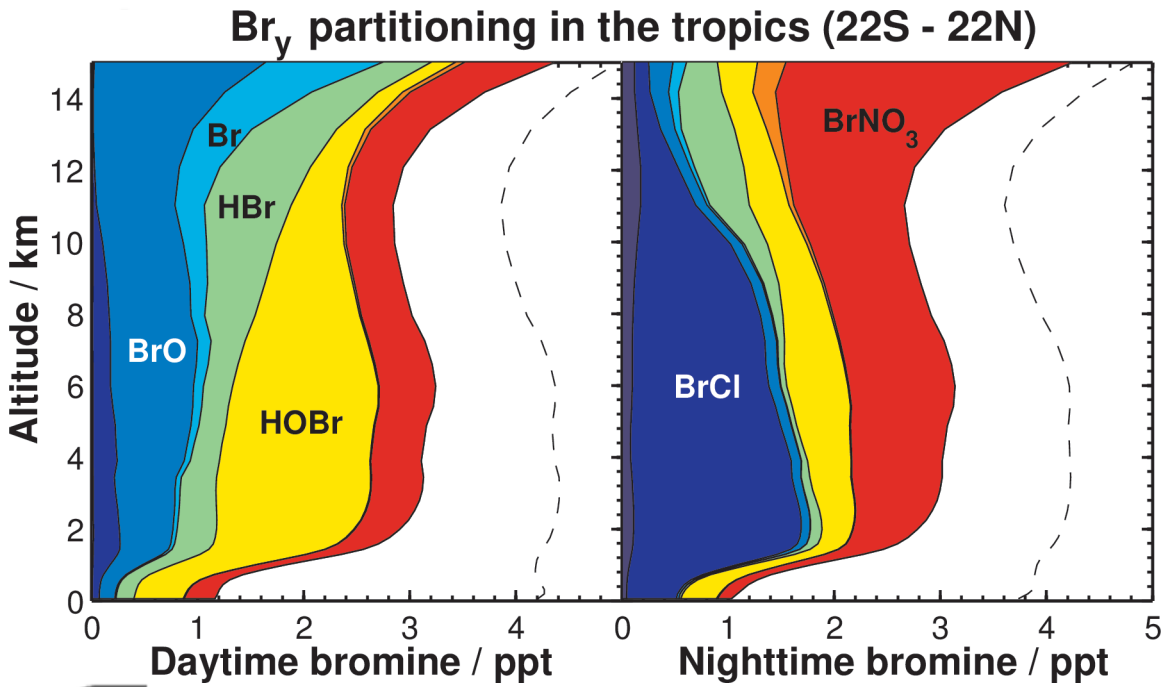

2015jd024229-f02-z-.eps

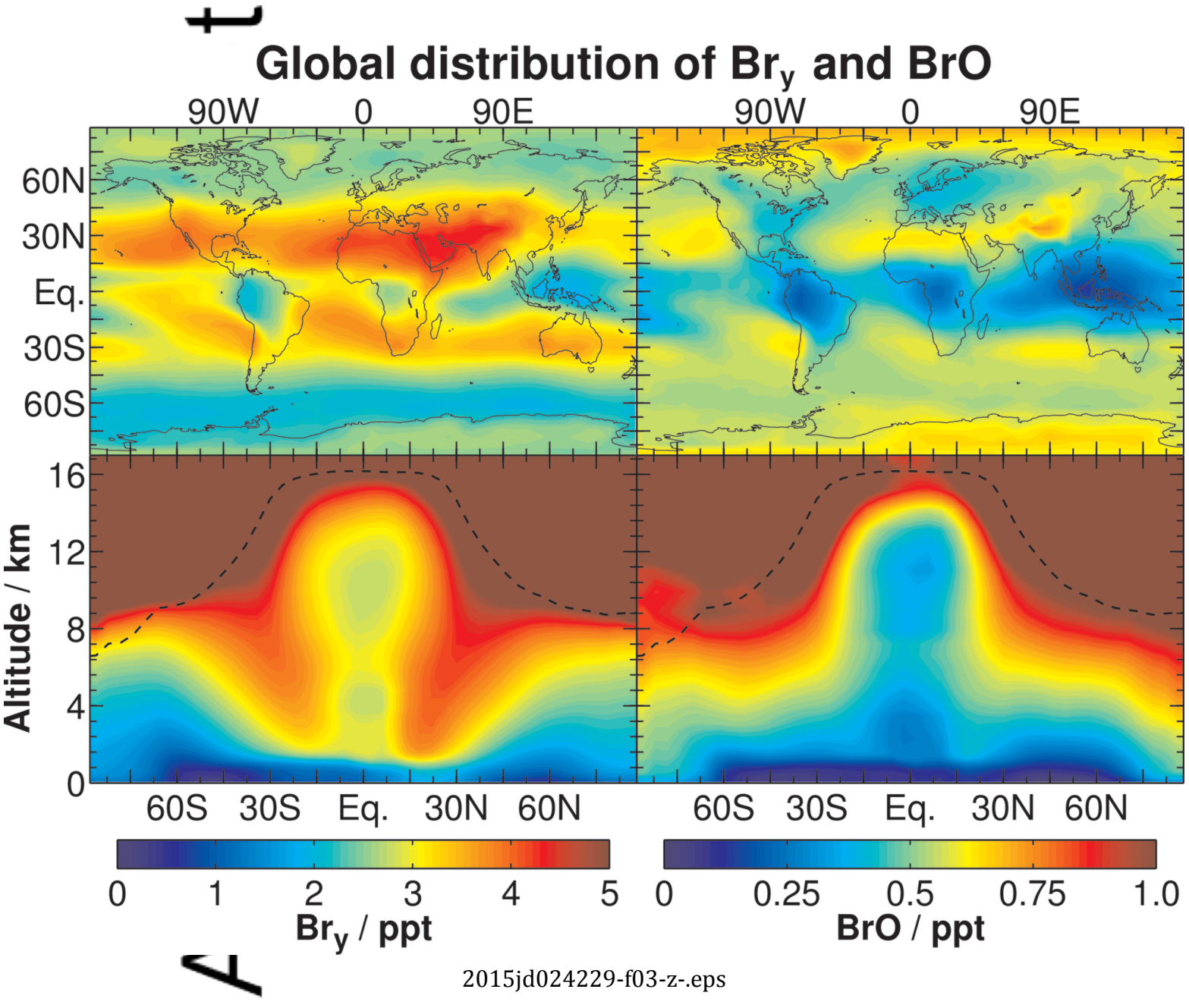

2015jd024229-f03-z-.eps

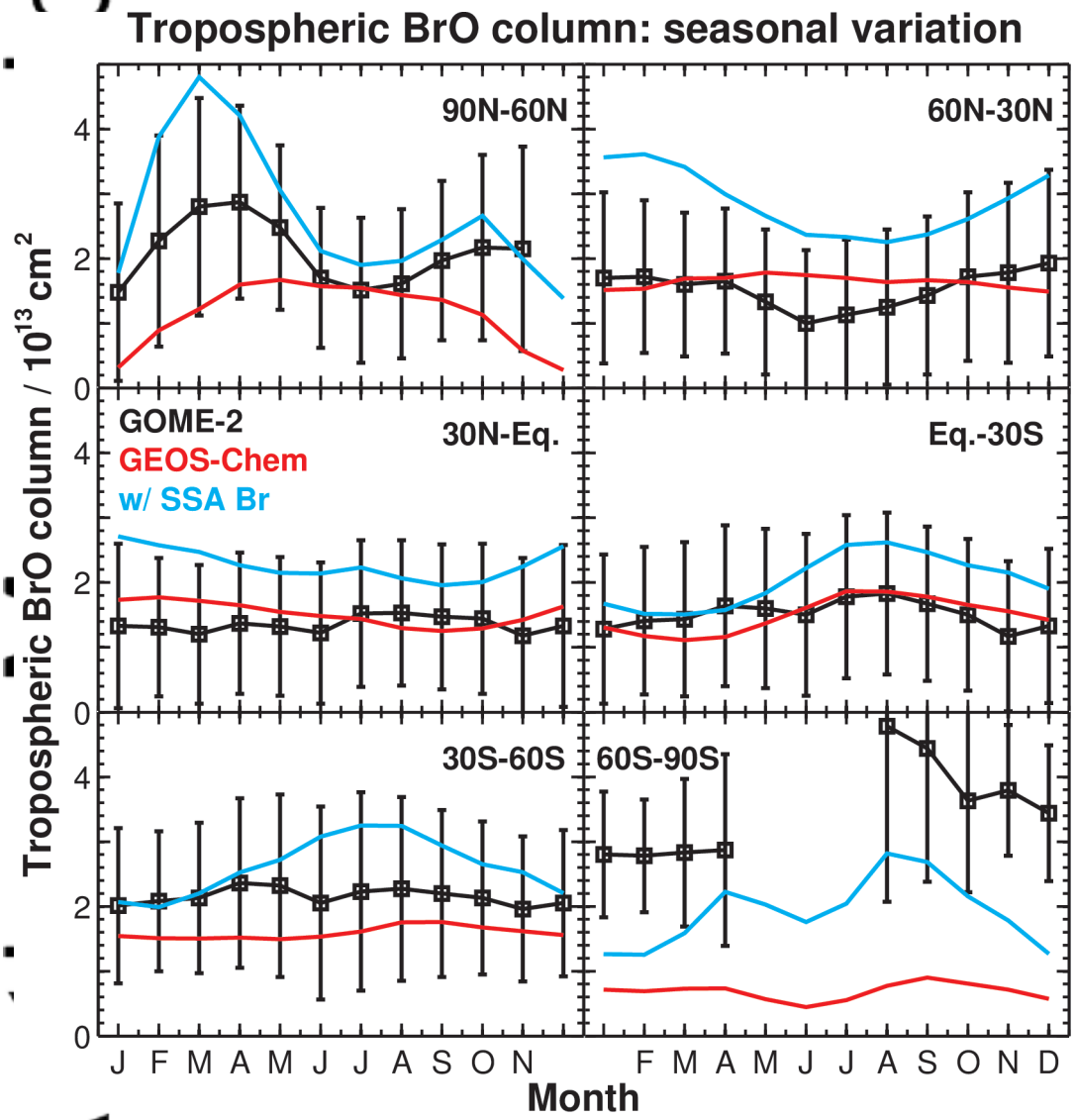

2015jd024229-f04-z-.eps

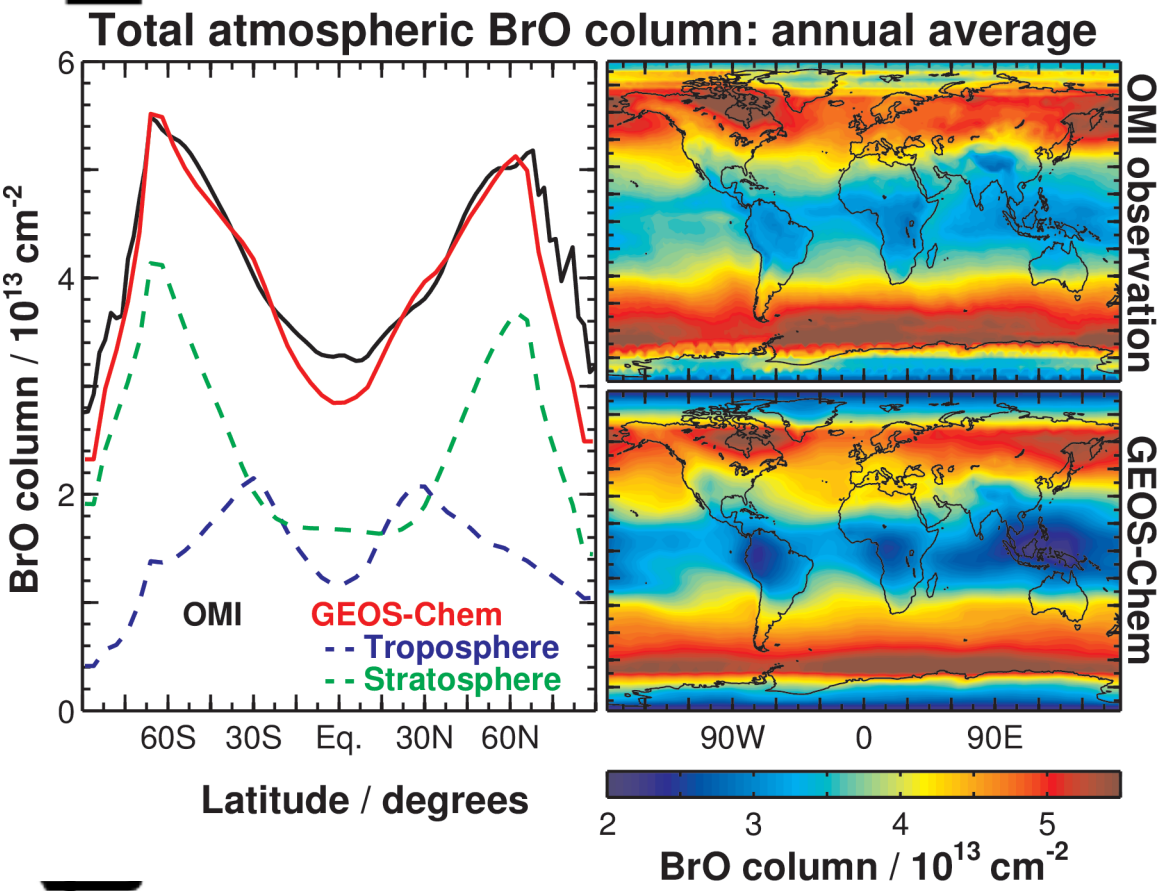

2015jd024229-f05-z-.eps

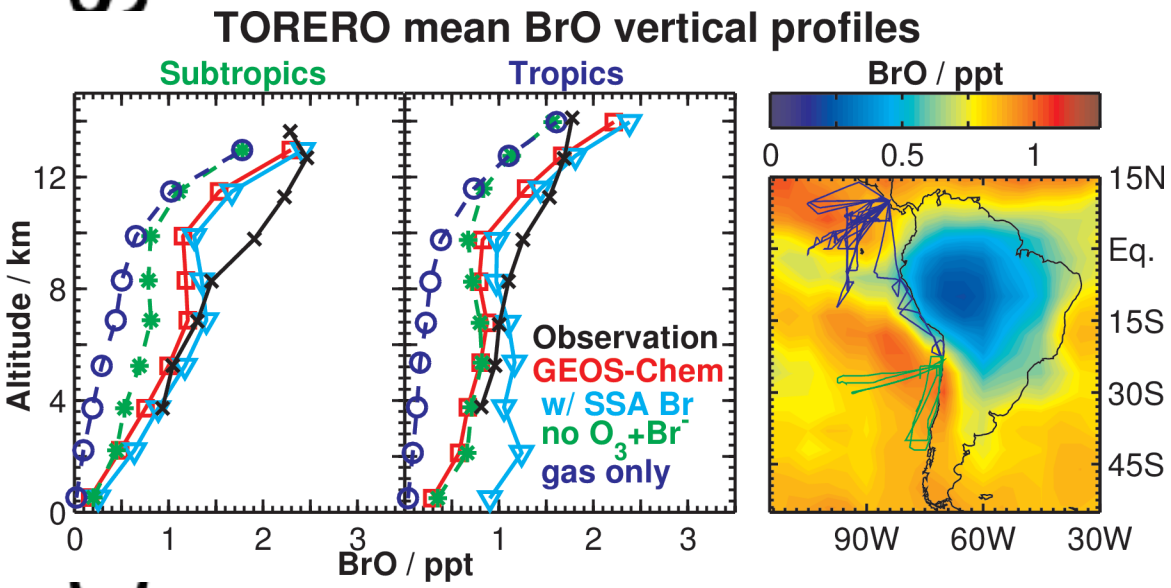

2015jd024229-f06-z-.eps

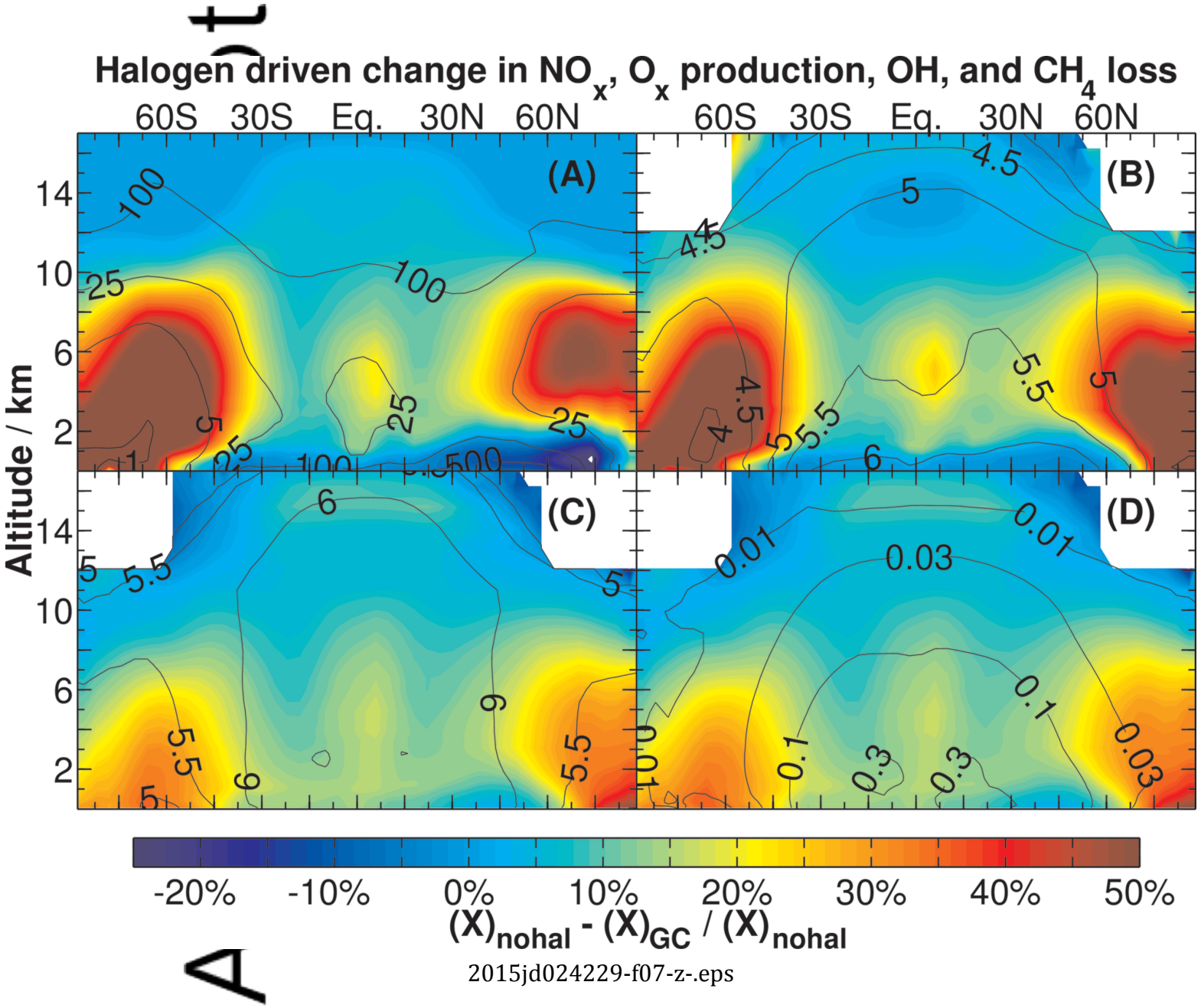

2015jd024229-f07-z-.eps

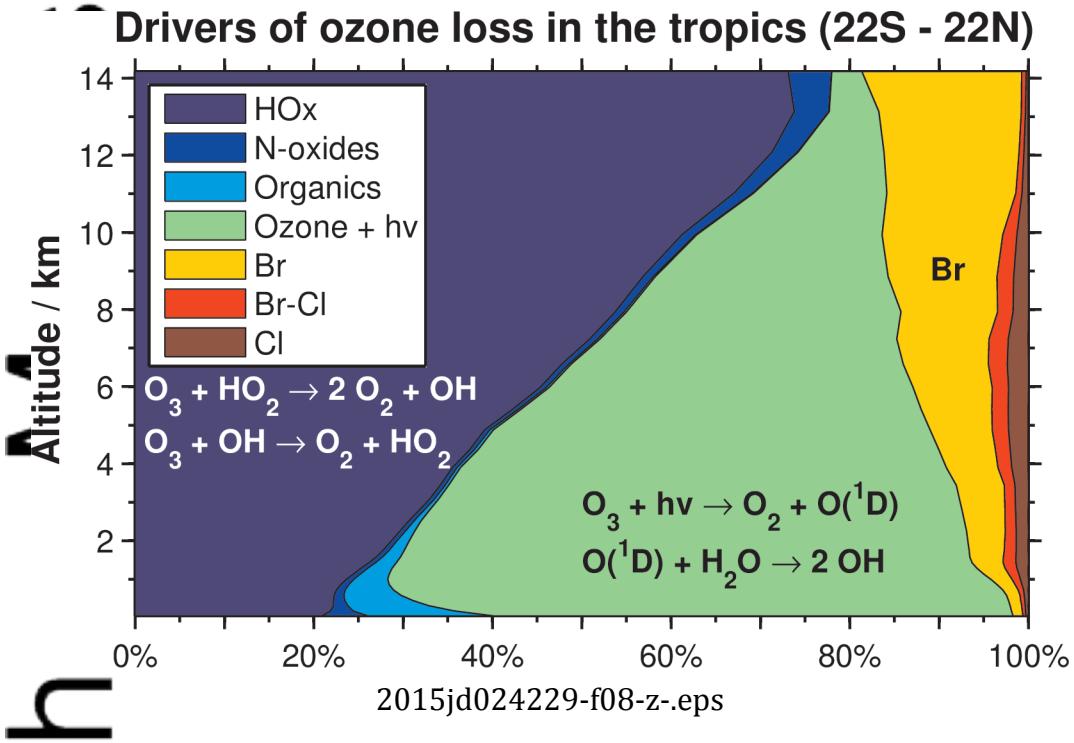

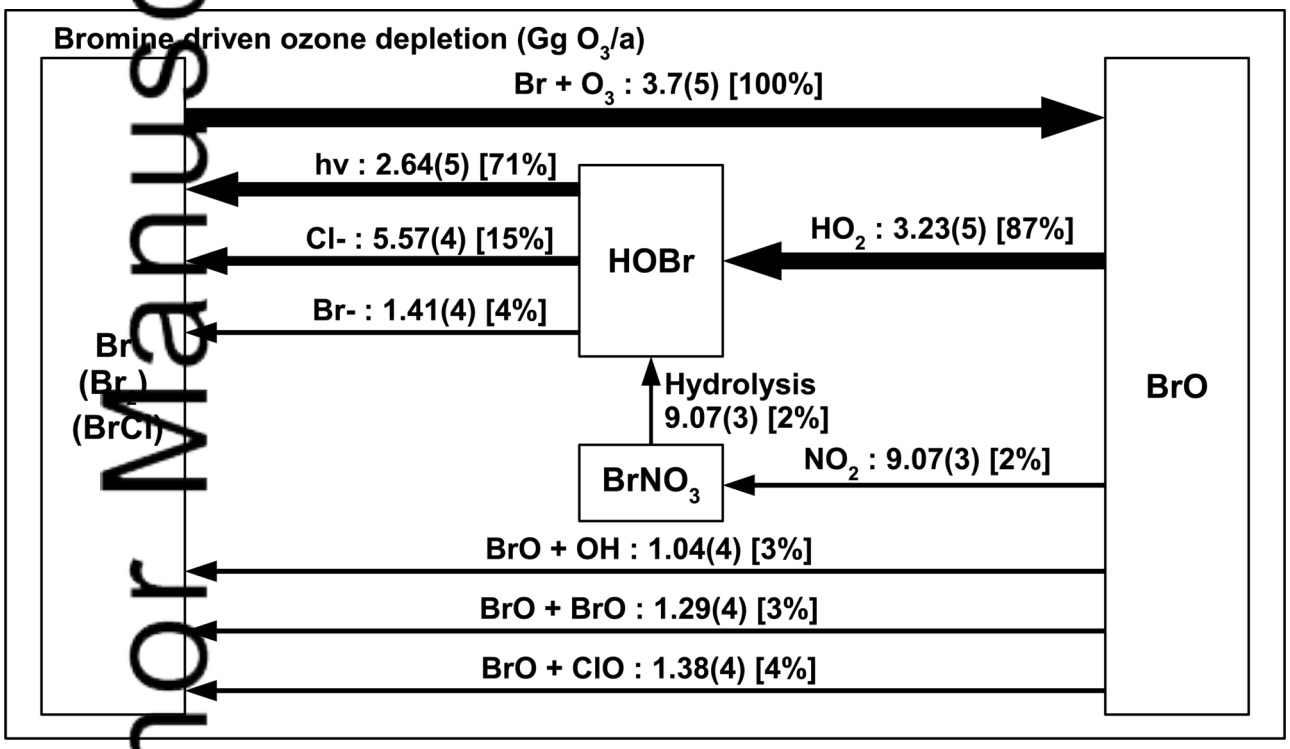

2015jd024229-f09-z-.eps

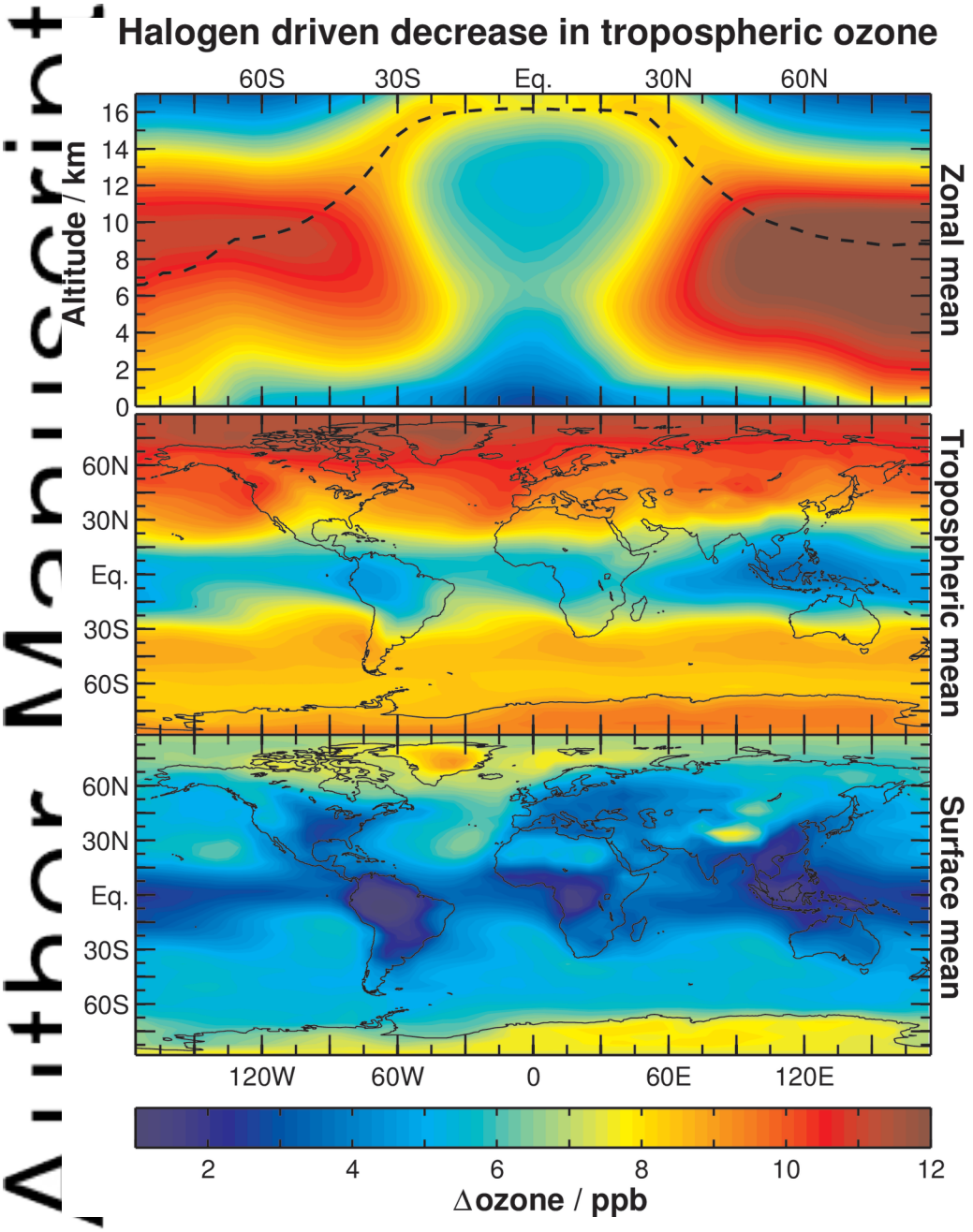

2015jd024229-f10-z-.eps

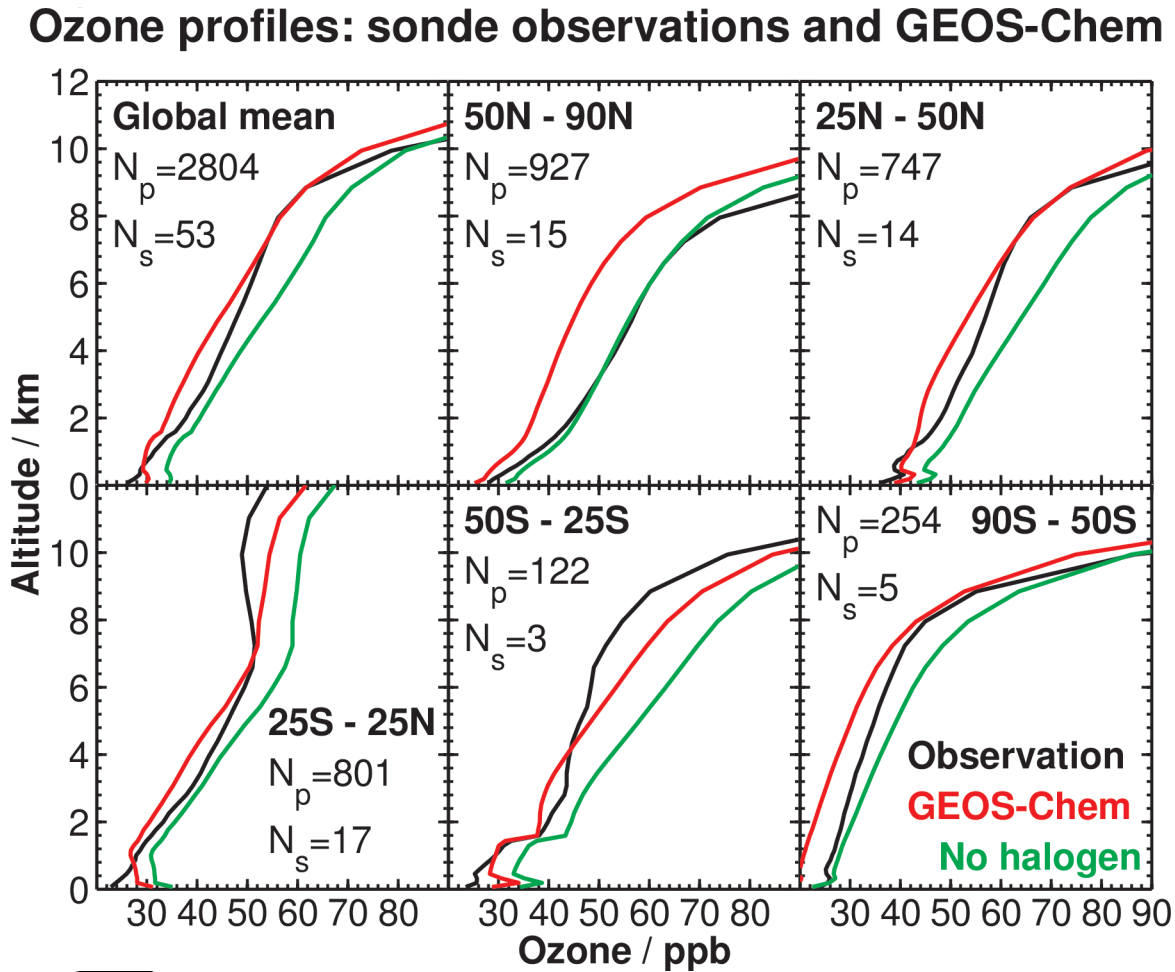

2015jd024229-f11-z-.eps

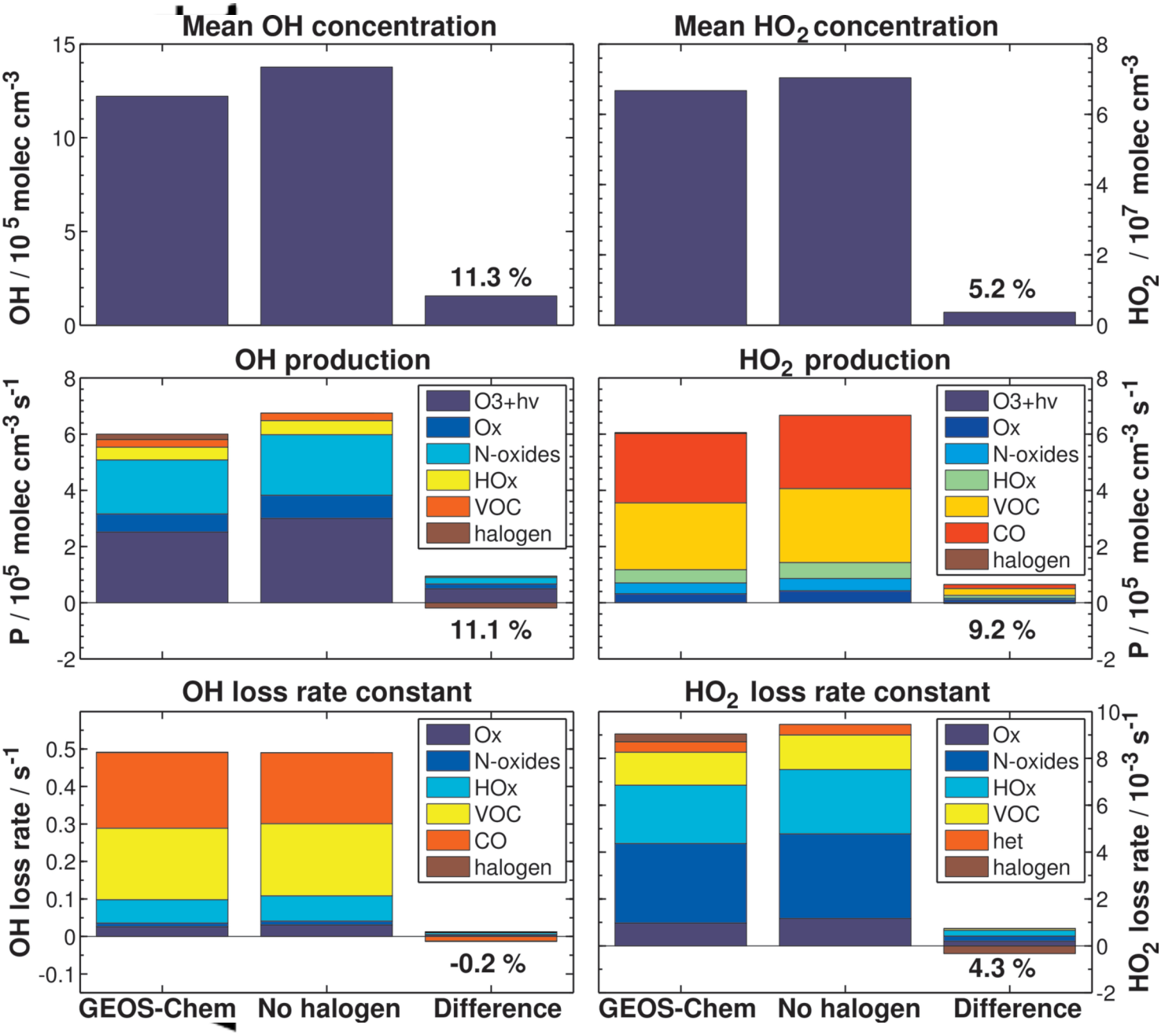

2015jd024229-f12-z-.eps